

**POLITECNICO**  
**MILANO 1863**

---

## FLASH

---



## Launch Systems Final Report

Name	Student ID	Email
Ahmed Loai Walid	10824003	loaiwalid.ahmed@mail.polimi.it
Gatto Agnese	10700799	agnese.gatto@mail.polimi.it
Gueli Gaetano	10725548	gaetano.gueli@mail.polimi.it
Martin Mihnea Stefan	10903720	mihneastefan.martin@mail.polimi.it
Martinez Ferreira Daniel	10887367	daniel.martinez@mail.polimi.it
Nys Clara	10972249	clara.nys@mail.polimi.it
Torre Federico	10645141	federico.torre@mail.polimi.it
Vetralla Davide	10683867	davide.vetralla@mail.polimi.it
Zara Andrea	10698650	andrea.zara@mail.polimi.it

**Course of Launch Systems  
School of Industrial Engineering  
Academic Year 2023-2024**

## **Abstract**

The purpose of this report is to present the design of the Fast Logistics Across Suborbital Highways (FLASH) ultra-fast transoceanic delivery service, predicated upon the specifications provided by customers. These requirement, includes time-to-market, maximum acceleration, payload mass, and arrival site,safety of the disposal of the stage , safety on ground serve as the foundational criteria for the Conceptual Design. First of all, a baseline is established through the analysis of the House of Quality (HOQ) , starting from the customer requirements and the quality characteristic to be achieved. The study proceed with the mission analysis to fix the mission's main features. The rocket can be then design: Dimensions, Aerodynamics, Propulsion, Recovery, and Weight are evaluated. Finally, the performance evaluation of the rocket with its nominal trajectory is provided; an analysis on how the possible launch uncertainties can affect the impact point was also carried out, utilizing a Montecarlo analysis. Upon completion of the preliminary design and definition of the mission profile, a preliminary requirements review is conducted to assess whether the customer's requirements are met by the obtained results.

# Nomenclature

Nondimensional Quantities				
$\epsilon$	Expansion Ratio	$A_{fairing}$	Fairing Area	[m <sup>2</sup> ]
$C_D$	Drag coefficient	$A_{fins}$	Fins Area	[m <sup>2</sup> ]
$C_N$	Normal coefficient	$c^*$	Characteristic velocity	[m/s]
$FOS$	Factor of Safety	$g_0$	Acceleration due to gravity at mean sea level	[m/s <sup>2</sup> ]
$n_{fins}$	Number of fins	$h_{gt}$	Gravity turn starting altitude	[km]
$L/D$	Fineness ratio	$K$	Thermal Conductivity	[W/mK]
$L_N/D_N$	Nose fineness ratio	$M$	Bending Moment	[Nm]
$M$	Mach number	$m$	Rocket mass	[kg]
Physical Quantities		$M_0$	Initial Mass Assumption	[kg]
$\Delta\gamma_{0,3}$	Change in the flight path angle between the end of the second stage and beginning of the third stage burn [rad]	$M_{av}$	Avionics Mass	[kg]
$\Delta v$	Velocity	$M_{engine}$	Engine Mass	[kg]
$\gamma$	Flight path angle	$M_{fairing}$	Fairing Mass	[kg]
$\gamma_0$	Initial flight path angle	$M_{fins}$	Fins Mass	[kg]
$\mathbf{r}_0$	Position vector of the launch site (ECEF)	$M_{nose}$	Nose Mass	[kg]
$\mathbf{r}_0$		$M_{nozzle}$	Nozzle Mass	[kg]
$\mathbf{r}_0$		$M_{T-Struct}$	Thrust Structure Mass	[kg]
$\mathbf{r}_f(t_{land})$	Position vector of the landing site (ECEF) as a function of the time of flight [km]	$M_{wiring}$	Wiring Mass	[kg]
$\omega$	Angular position along the trajectory [rad]	$p$	Internal Pressure	[m <sup>2</sup> ]
$\rho_{air}$	Air density [kg/m <sup>3</sup> ]	$P_e$	Nozzle exit pressure	[Pa]
$\rho_m$	Material density [kg/m <sup>3</sup> ]	$P_{atm}$	Ambient pressure	[Pa]
$\sigma_y$	Material Yielding Stress [Pa]	$p_c$	Combustion Pressure	[Pa]
$\theta_{cn}$	Half Angle [rad]	$r$	Distance from Earth's center	[km]
		$R_E$	Earth radius	[km]
		$S_{LateralNoz}$	Lateral Surface of the nozzle	[m <sup>2</sup> ]
		$T$	Thrust	[N]

$T_0$	Thrust at optimal altitude	[N]	$v$	Velocity	[m/s]
$t_{b,3}$	Burning time of the third stage	[s]	$x_{CG}$	Center of gravity position from the nose tip of the rocket	[m]
$T_{max-admiss}$	Maximum Admissible Temperature	[C°]	$x_{CP}$	Center of pressure position from the nose tip of the rocket	[m]
$th$	Structure thickness	[mm]			
$th_{BendMoment}$	Maneuver Bending Moment contribution to body structure thickness	[mm]	$A_e$	Nozzle exit area	[m <sup>2</sup> ]
$th_{BuckAxial}$	Localized Buckling in Axial Compression	[mm]	$A_{nose}$	Cross section of the circle describing the bluntness	[m <sup>2</sup> ]
$th_{BuckBend}$	Localized Buckling in Bending	[mm]	$A_{ref}$	Aerodynamic reference area	[m <sup>2</sup> ]
$th_{fins}$	Fins thickness	[mm]	$b$	Span	[m]
$th_{Gauge}$	Minimum Gauge for manufacturing	[mm]	$D$	Body diameter	[m]
$th_{nose}$	Nose thickness	[mm]	$E$	Material Modulus of Elasticity	[Pa]
$th_{nose}$	Nose thickness	[mm]	$L$	Body length	[m]
$th_{pressure}$	Internal Pressure contribution to body structure thickness	[mm]	$L_n$	Nose length	[m]
$th_{Thrust}$	Thrust force contribution to body structure thickness	[mm]			

**Abbreviations**

$C_G$	Center of gravity
$C_P$	Center of pressure

## Acronyms

<b>ANSP</b>	Air Navigation Service Provider	<b>HOQ</b>	House of Quality
<b>AST</b>	Office of Commercial Space Transportation	<b>HTPB</b>	Hydroxyl-Terminated Polybutadiene
<b>CEA</b>	Chemical Equilibrium Applications	<b>LRE</b>	Liquid Rocket Engine
<b>EASA</b>	European Aviation Safety Agency	<b>LSC</b>	Linear Shaped Charge
<b>FAA</b>	Federal Aviation Administration	<b>PID</b>	Proportional-Integral-Derivative
<b>FLASH</b>	Fast Logistics Across Suborbital Highways	<b>PSLV</b>	Polar Satellite Launch Vehicle
<b>FLSC</b>	Flexible Linear Shaped Charges	<b>SRM</b>	Solid Rocket Motor
<b>FTS</b>	Flight Termination System	<b>TPS</b>	Thermal Protection System
<b>GNC</b>	Guidance, Navigation and Control	<b>TRL</b>	Technology Readiness Level
<b>GSLV</b>	Geosynchronous Satellite Launch Vehicle	<b>TVC</b>	Thrust Vector Control

# Contents

<b>1</b>	<b>Introduction</b>	<b>1</b>
<b>2</b>	<b>Project Management</b>	<b>2</b>
2.1	House of Quality . . . . .	2
2.1.1	Pareto Analysis . . . . .	2
2.1.2	Competitors Analysis . . . . .	3
2.1.3	Costs analysis and business plan . . . . .	3
2.2	Baseline . . . . .	4
2.3	Legislation on Suborbital Flights . . . . .	4
2.4	Choice of Launching and Landing Sites . . . . .	5
<b>3</b>	<b>Design</b>	<b>6</b>
3.1	Staging . . . . .	6
3.2	Dimensions . . . . .	6
3.3	Aerodynamics . . . . .	7
3.3.1	Drag Coefficient . . . . .	7
3.3.2	Normal Force . . . . .	9
3.3.3	Re-entry . . . . .	10
3.3.4	Stability . . . . .	12
3.4	Structure Analysis . . . . .	13
3.4.1	Structural Verification . . . . .	15
3.5	Propulsion . . . . .	17
3.5.1	Propellant . . . . .	18
3.5.2	Motor Modification and Design . . . . .	19
3.5.3	Stage Separation Systems . . . . .	20
3.6	Trajectory . . . . .	21
3.6.1	Models . . . . .	21
3.6.2	Implementation . . . . .	21
3.6.3	Nominal trajectory simulation . . . . .	22
3.6.4	Monte Carlo analysis . . . . .	22
3.7	Guidance . . . . .	23
3.8	Atmospheric re-entry and landing . . . . .	24
3.8.1	Parachutes sizing . . . . .	24
3.8.2	Thermal analysis . . . . .	26
<b>4</b>	<b>TRL and Client Requirements</b>	<b>29</b>
4.1	TRL and AD <sup>2</sup> . . . . .	29
4.1.1	Engines . . . . .	29
4.1.2	Materials . . . . .	29
4.1.3	Fins . . . . .	30

4.1.4	Capsule . . . . .	30
4.1.5	Parachute . . . . .	30
4.1.6	Control System . . . . .	30
4.2	Client requirements . . . . .	30
4.2.1	Ready within hours . . . . .	30
4.2.2	Safety on ground . . . . .	30
<b>5</b>	<b>Conclusion</b> . . . . .	<b>31</b>
5.1	Project Management Appendix . . . . .	32
5.2	Staging Appendix . . . . .	39
5.3	Aerodynamics Appendix . . . . .	40
5.4	Structure Appendix . . . . .	45
5.5	Propulsion Appendix . . . . .	46
5.6	Dimensions Appendix . . . . .	47
5.7	Trajectory Appendix . . . . .	48
5.8	Atmospheric re-entry and landing Appendix . . . . .	52
5.9	Guidance Appendix . . . . .	55

# List of Figures

3.1	Main models and assumptions used to obtain aerodynamics coefficients and forces depending on the phase considered . . . . .	7
3.2	Drag coefficient and force dependence on M and altitude . . . . .	8
3.3	Normal coefficient and force dependence on $\alpha$ and altitude at $M = 2$ . . . . .	9
3.4	Drag and Lift coefficients and force dependence during reentry . . . . .	10
3.5	Normal coefficient and force dependence during reentry . . . . .	11
3.6	Lift and Drag coefficient ascent phase . . . . .	12
3.7	Drag coefficient vs Knudsen Number . . . . .	12
3.8	Center of gravity, center of pressure and static margin stability (distance from rocket tip) for a specific ballisitic trajectory . . . . .	13
3.9	Axial Forces . . . . .	14
3.10	Maximum Bending Moments . . . . .	14
3.11	Impact Area . . . . .	16
3.12	Propulsion system functional analysis . . . . .	17
3.13	Montecarlo analysis for West landing site . . . . .	23
3.14	$\dot{q}_{tot}$ over time . . . . .	27
3.15	Ablation temperature over time . . . . .	28
5.1	Mission concept synthesis requires evaluation of alternatives (alt.) and iterations, from [5] . . . . .	32
5.2	House of quality sheet . . . . .	33
5.3	Optimal staging analysis . . . . .	39
5.4	Temperature, density and gravity variation with altitude . . . . .	40
5.5	Pressure coefficients for Newton and modified Newton . . . . .	41
5.6	Normal vector forces . . . . .	42
5.7	Normal forces during reentry . . . . .	42
5.8	Relation between Depth of penetration, Caliber and Standoff distance [14] . .	45
5.9	1 <sup>st</sup> stage nozzle before (left) and after (right) the modification . . . . .	46
5.10	3 <sup>rd</sup> stage propulsion system: starting from left, the collet mechanism (1), the pressurising gas tank, oxidiser tank, fuel tank, combustion chamber and nozzle are shown in this order, together with their sizes. . . . .	46
5.12	Time history for the ascent phase of the West Coast trajectory . . . . .	48
5.13	Time history for the descent phase of the West Coast trajectory . . . . .	48
5.14	Time history for the ascent phase of the Midwest trajectory . . . . .	49
5.15	Time history for the descent phase of the Midwest trajectory . . . . .	49
5.16	Time history for the ascent phase of the East Coast trajectory . . . . .	50
5.17	Time history for the descent phase of the East Coast trajectory . . . . .	50
5.18	Trajectory simulation for each landing site . . . . .	51
5.19	Tabulated $C_D$ and $C_X$ values [29] . . . . .	52
5.20	Parachute diameter and mass correlation [29] . . . . .	52

5.21 Canopy Fill constant $n$ for Various Parachutes Types [29] . . . . .	53
5.22 Opening-Force Reduction Factor $X$ Versus Ballstic Parameter $A$ [29] . . . . .	53
5.23 Montecarlo analysis for West landing site . . . . .	54
5.24 Montecarlo analysis for West landing site . . . . .	54
5.25 Reference Frame . . . . .	56
5.26 Control Evolution . . . . .	56

# List of Tables

2.1	Quality functions and their relative weights . . . . .	3
2.2	Competitors . . . . .	3
2.3	Total Cost . . . . .	4
2.4	Business Plan . . . . .	4
3.1	Physical parameters obtained from the CAD model . . . . .	7
3.2	Considered Material . . . . .	15
3.3	Masses . . . . .	16
3.4	SRM original and LRE expected properties. . . . .	18
3.5	Tuned solid boosters parameters and final Liquid Rocket Engine (LRE) design parameters. The Solid Rocket Motor (SRM) diameters are different due to the inclusion and/or modification of structural components. . . . .	19
3.6	Optimization results . . . . .	22
3.7	Montecarlo Analysis on the Range . . . . .	23
3.8	PID law . . . . .	24
3.9	Drogue and main parachutes data . . . . .	25
3.10	Recovery results . . . . .	25
3.11	Ablative material's properties and resulting thicknesses and masses . . . . .	27
4.1	Technology Readiness Level (TRL) table summary . . . . .	29
5.1	Requirements Fulfilment . . . . .	31
5.2	Values of baselines for each stage . . . . .	34
5.3	TRL criteria table [10] . . . . .	34
5.4	AD <sup>2</sup> criteria table [10] . . . . .	35
5.5	Fixed costs . . . . .	36
5.6	Recurrent costs . . . . .	37
5.7	Total Recurrent costs . . . . .	38
5.8	Launches Price . . . . .	38
5.9	NCF and NPV . . . . .	38

# Chapter 1

## Introduction

FLASH is a three-stage rocket with the capability of transporting payloads ranging from 10 to 100 kg from Europe to the United States in less than one hour. A capsule equipped with a parachute recovery system ensures the safe retrieval of the payload without sustaining damage.

Throughout the preliminary design phase, each design choice and the trade-offs between two potential launch sites—Andøya in Sweden and Harstad in Norway—have been carefully evaluated. This evaluation was conducted to facilitate payload delivery to three distinct landing sites on the USA's East Coast (Atlantic Ocean), West Coast (Utah's Desert), and the Midwest (Lake Superior).

The design process is significantly influenced by the customer's requirement for a high TRL. To meet this requirement, a delicate balance between various technologies has been struck, involving trade-offs to optimize the overall design and ensure the successful accomplishment of the mission 5.6.



# Chapter 2

## Project Management

The initial design activities undertaken pertain to Phase 0, which is dedicated to acquiring precise data concerning mission objectives and technical specifications. Concurrently, Phase A 5.1 has as its principal objectives the formulation of a comprehensive system architecture and the development of an operational concept.

### 2.1 House of Quality

Understanding customer needs is foundational to the design process. The HOQ plays a pivotal role in this initial phase by elucidating the relationships between requirements and technical aspects. Analyzing the HOQ depicted in Figure 5.2, we can discern the optimal approach to addressing the identified problem.

The HOQ serves as a roadmap during the launcher design process, considering various launchers for both in-orbit and ballistic missile applications (refer to Appendix 5.1 for details). The primary goal of the HOQ is to provide a comprehensive overview of technologies that can support our sizing requirements, for example including both liquid and solid engine launcher. This aspect will be further clarified in Chapter 3.5, where the chosen propulsion technology for the final three-stage rocket is discussed.

The HOQ sheet is structured by first addressing client requests, as outlined on the left side in the figure provided in the appendix. Following this, the importance of primary design drivers is characterized. The right side of the HOQ is then meticulously dedicated to the analysis of competitor data, providing a comprehensive perspective on the design landscape 5.1.

#### 2.1.1 Pareto Analysis

In order to discern the technical parameters that wield the most significant influence in meeting the requirements, a Pareto 80-20 analysis is conducted.

Quality Function	Relative Weight
Safety factor	14.1%
Failure probability	14.1%
Landing uncertainty	14%
Toxicity index	8.1%
Thrust over Weight Ratio	7.8%
$\Delta v$	7.2%
Cost of the mission	6.9%
Thrust	6.9%
Range	5.1%
$L/D$	4.5%
Volume of fairing	4.1%
Latitude of Launch site	2.9%
Structural mass index	2.8%
$C_D$	1.5%

Table 2.1: Quality functions and their relative weights

In accordance with Pareto's law, the threshold of 80% is obtained by summing the relative weights of the highlighted quality functions presented in Table 2.1. Consequently, these functions emerge as the most crucial parameters to prioritize during the design phase.

### 2.1.2 Competitors Analysis

The HOQ helps to figure out the competitiveness of the designed rocket; in Table 2.2 are summarized the overall scores of the competitors against FLASH.

FLASH	Minuteman II	Falcon I	Vega C	Ariane V	Agni Series
34	27	24	26	25	22

Table 2.2: Competitors

As evident, FLASH exhibits competitiveness in comparison to other vehicles. The competitors are then scrutinized to establish a baseline for our rocket's design. Notably, not every analyzed vehicle is explicitly designed for an intercontinental flight. Consequently, even accounting for the high grade assigned to the Minuteman III mission in the analysis, it is adopted as the baseline.

### 2.1.3 Costs analysis and business plan

A cost analysis of the mission was carried out following a down-top estimation approach [1]. Results were then validated through a top-down estimation method, comparing them to past similar mission. For the purpose of this analysis, which specification are shown in Appendix 5.1, a differentiation between Fixed and Recurrent Costs is done. By summing up all the work package costs, subdivided in direct and indirect costs, and including a risk insurance cover for the scientific payload, the Total Cost has been computed as the sum of fixed, manufacturing and operations contributions, as shown in the Table 2.3

<b>Manufacturing</b>	55.577.515,72 €
<b>Operational</b>	620.000,00 €
<b>Fixed</b>	9.903.900,00 €
<b>Total Costs per Launch</b>	66.287.415,72 €

Table 2.3: Total Cost

A business plan is also developed. According to a brief market analysis, a competitive launch price, the number of launches per year and number of years of activity were established in order to make our company competitive in the market and understand if the investment to be done on the rocket is worthy. The results can be seen in Table 2.4

Launch per Year	Years of Activity	Launch price
15	10	150.500.000,00 €
Net Present Value	Return on Investment	Payback Time
15.055.720.005,62 €	37,52%	3 years

Table 2.4: Business Plan

## 2.2 Baseline

The **LGM-30G Minuteman III** is a three-stage, solid-fueled, intercontinental-range ballistic missile, constituting the exclusive land-based component of the U.S. nuclear triad. It is renowned for its swift launch time, nearly 100 percent testing reliability, and backup airborne launch controllers, ensuring the preservation of retaliatory capabilities [2]. This mission serves as an excellent baseline due to its extensive experience background. Development of the Minuteman III commenced in 1966 as an improvement program for earlier Minuteman missile systems. It successfully underwent its inaugural flight test in 1968 and achieved operational status two years later [3].

The Minuteman III missile boasts a maximum range of 13,000 km and is capable of carrying a payload of three reentry vehicles. It measures 18.2 m in length, has a diameter of 1.85 m, and a launch weight of 34,467 kg [2].

The results obtained from the HOQ provide the path to achieving the mission objective. The most suitable rocket identified is the **Minuteman III**, a military rocket capable of high  $\Delta V$  with three solid engines. The FLASH rocket is designed by incorporating taking in account reference data from Minuteman III, the data considered are shown in Appendix 5.2.

The results obtained from the HOQ define the trajectory towards accomplishing the mission objective. Among the discerned options, the most viable rocket is the **Minuteman III**—a military-grade rocket renowned for its capability to achieve high  $\Delta V$  through the deployment of three solid engines. The FLASH rocket's design is intricately shaped by referencing data from the Minuteman III. The specific design parameters are outlined in Appendix 5.2.

## 2.3 Legislation on Suborbital Flights

In order to conduct intercontinental rocket flights, strict safety rules must be observed. Designated forbidden regions influence the choice of lift-off sites and landing site, as discussed in Section 2.4.

While there is no specific legislation for suborbital intercontinental flights, regulations generally fall under broader categories related to aviation, aerospace, and space transportation. Key differences exist between European and U.S. regulatory bodies, particularly in air

traffic permissions. The European Aviation Safety Agency (EASA) focuses on civil aviation safety, with discussions about a specific regulatory framework for space activities. The EU draft space regulation addresses licensing, safety, environmental protection, and insurance for space activities, working in coordination with national authorities.

For this project, the spaceport is considered a partner responsible for adhering to European legislation. Spaceport legislation is not discussed further in this paper. In contrast, the Federal Aviation Administration (FAA) in the U.S. has specific regulations for suborbital space activities. The FAA's Office of Commercial Space Transportation (AST) regulates and licenses commercial space operations, including suborbital flights. Operators must document environmental and population impacts, implement hazard mitigation protocols, and undergo inspections by the Department of Transportation.

## 2.4 Choice of Launching and Landing Sites

For the choice of the launching site, several locations have been considered, throughout the western and central part of Europe. The key criteria involve minimizing both the distance to be traveled and velocity losses. Additionally, a crucial consideration in site selection is to avoid launching towards densely populated areas for safety reasons. Another aspect influencing the choice of the launch site is the connectivity from a logistical perspective, ensuring that the site is easily accessible by car or plane. The final factor in selecting the launch site is the air congestion level and the presence of existing regulations for rocket launches provided by the Air Navigation Service Provider Air Navigation Service Provider (ANSP).

Considering all factors, the two sites that appeared most suitable were Kiruna, Sweden, and Andøya, Norway. Ultimately, the site chosen was Andøya, as it was deemed more favorable. This decision was influenced by its proximity to the Atlantic Ocean compared to Kiruna, reducing the chances of passing over populated areas, such as the city of Narvik.

Landing site for the flight to the East Coast was considered the Atlantic Ocean. This was considered as it provides a higher level of safety than landing on ground, as having a smaller impact on the population and on the landing. For the landing site in the Middle-West area, it was considered better to proceed with a water landing in the Greater Lakes. As Lake Michigan has a smaller surface, by 30%, compared to Lake Superior, the last was chosen. Furthermore, the population around the Lake Superior is comparatively smaller than around Lake Michigan, about 5% of the population. The drawback presented at water landing is the effect of water on the vehicle's body, affecting thus the level of re-usability of the rocket. While for the West coast it was taken as landing site the Mojave Desert. This selected region presents a low level of populations and also a position where the recovering of the rocket is more accessible.

# Chapter 3

## Design

This chapter delves into the comprehensive criteria for sizing the launcher. In-depth studies are conducted on aerodynamics, propulsion, structure, trajectory, and guidance to ensure the completion of the preliminary design. Towards the conclusion of this chapter, a TRL analysis is performed to verify that our design aligns with the customer's requirements.

### 3.1 Staging

By applying the Tsiolkovsky equation, we initially estimate the total mission budget. The transition from the baseline to our rocket is accomplished by calculating the specific impulse of the new propellant, adjusted by the degradation factor  $\eta$  obtained from the baseline, as defined in Appendix 5.2. The procedure employed to define the staging involves an optimization process aimed at minimizing the launcher's mass while achieving the desired  $\Delta v$ . The minimization function  $J$ , detailed in Appendix 5.2, guides this process. As depicted in the Figure in Appendix 5.2, the optimal number of stages for the FLASH mission is determined to be three. Further insights into the impracticality of the other two analyzed solutions are presented in Figure 5.3, where the masses are observed to be excessively high.

### 3.2 Dimensions

In order to correctly simulate the rocket's dynamics for the control loop design (see Section 3.7), a CAD model of FLASH was created. This model includes the mass and position of the major components of the rocket in order to have an accurate estimation of the  $C_G$  position and inertia moments, mainly. Table 3.1 shows the relevant physical parameters for each stack. The general dimensions of the rocket and the capsule can be seen in Appendix 5.6

Flight phase	$I_1 [kgm^2]$	$I_2 = I_3 [kgm^2]$	Stack mass [kg]	Stack length [m]	$C_G$ position [m]
Launch	2411.923	490098.445	17735	19.5622	11.5158
Stage 1 burnout	996.35	180219.81	7760		7.2268
Stage 2 fire	571.741	46502.685	5965	9.4732	4.5388
Stage 2 burnout	414.321	21861.62	4024		3.1548
Stage 3 fire	312.429	8195.942	3436	6.3753	2.689
Stage 3 burnout	132.109	5824.043	1151		2.51
Capsule	22.807	19.29	331	0.7	0.467
Notes	Roll	Pitch/yaw			Measured from the tip of the rocket

Table 3.1: Physical parameters obtained from the CAD model

### 3.3 Aerodynamics

Two different approaches have been used to analyze and optimize aerodynamics forces. The first is based on breaking down the rocket into separate elements, summing up their contributions ("components buildup"). The second uses the paneling method to calculate the pressure coefficient by dividing the total surface of our launcher into several panels, where the local effect is computed. Furthermore, the stability of the launcher was evaluated using OpenRocket. For proper aerodynamic analysis of the rocket, a model that accurately simulates the atmosphere was selected, the 1976 U.S. Standard Atmosphere [4]. This model enables the determination of temperature, air density, and gravity based on the geometric altitude as input, Appendix [5.3].

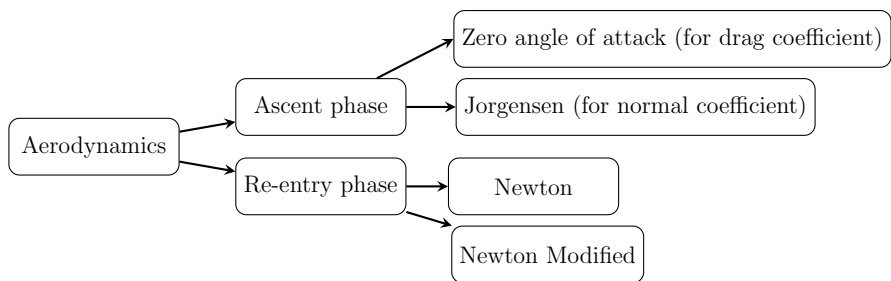


Figure 3.1: Main models and assumptions used to obtain aerodynamics coefficients and forces depending on the phase considered

#### 3.3.1 Drag Coefficient

The primary assumption made is that the angle of attack ( $\alpha$ ) is zero for calculating all drag coefficients, with the deviation in drag between the actual scenario and the  $\alpha = 0$  assumption being considered insignificant. The computation is performed considering separately the contribution given by the body and wings.

The zero lift drag coefficient of a symmetric body is due to three contributions :

- **Wave drag** : This drag type is exclusive to supersonic conditions ( $M > 1$ ). It's related to the impact of shock waves on an object, influenced by its pressure distribution. The analysis of this phenomenon employs the Bonney model [5], a simplified method particularly suited for sharp-nosed designs. To create a shape that is a blend between a sharp nose and a hemisphere, the design can integrate aspects of both forms by adjusting their respective influences according to the targeted design specification.
- **Friction drag** : This is the resistance caused by the air's viscous flow around the rocket, based on the premise of turbulent flow and the absence of a boattail. This assumes that the speed of sound and air viscosity don't vary significantly from the free stream at different altitudes. Additionally, this model simplifies by not being dependent on the Reynolds number ( $Re$ ).
- **Base drag** : This type of drag is a result of the pressure effects and is primarily influenced by the interaction between the airflow and the rocket's nozzle section. Base drag creates a low-pressure zone at the rocket's base or wherever the body radius decreases rapidly. This drag is less significant during powered flight but becomes more pronounced during unpowered flight phases.

The wings drag coefficient is due to two contributions : **wave drag** and **friction drag**, as detailed in Appendix 5.3 based on [5].

$$(C_{D0})_{\text{tot}} = (C_{D0})_{\text{body, wave}} + (C_{D0})_{\text{body, friction}} + (C_{D0})_{\text{base}} + (C_{D0})_{\text{surf, wave}} + (C_{D0})_{\text{surf, friction}} \quad (3.1)$$

Finally, the drag force is computed as:

$$D = q (C_{D0})_{\text{tot}} S_{ref} \quad (3.2)$$

The drag has been assessed for the three stages. The most critical stage in terms of drag is the first stage during its unpowered phase. Drag is directly proportional to air density, which is heightened at lower altitudes. Furthermore, the augmented surface area exposed to the flow amplifies the drag force.

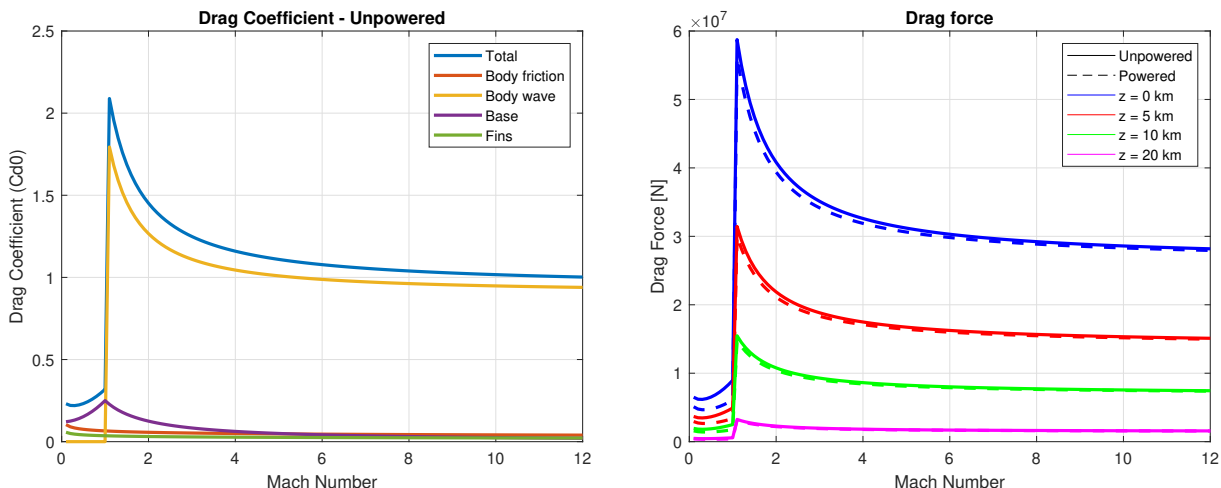


Figure 3.2: Drag coefficient and force dependence on  $M$  and altitude

The drag coefficient is high relative to the range expected for a rocket of this type. This deviation is primarily attributed to the predominant influence of wave drag, as illustrated in

Figure 3.2, a direct consequence of the nose's geometric profile ( $L_n/D_n$ ). In our case, the rocket is not equipped with a fairing but rather a capsule has been designed (see Section 3.8). The capsule's design is aerodynamically optimized for atmospheric re-entry, where a pronounced frontal angle serves three critical functions: it facilitates the thermal energy dissipation, enhances aerostatic stability during the descent trajectory, and augments the effectiveness of atmospheric deceleration. Conversely, this configuration is suboptimal for reducing drag during the ascent phase, where a design featuring an ogival shape with an extended length-to-diameter ( $L_n/D_n$ ) ratio would be more advantageous. However, when considering the overall trajectory (3.6), the choice to accept increased drag in this phase is justified by the benefits offered by this shape during other mission-critical stages (re-entry and descent).

### 3.3.2 Normal Force

The normal force coefficient ( $C_N$ ) is determined through an analysis of the effects from the elongated cylindrical body, which incorporates a nose cone, and the dual sets of trapezoidal fins. For the body's contribution, the Allen model for axially symmetric bodies is employed and an another term is added due to cross flow component  $V_r \sin(\alpha)$ . This computation assesses  $C_N$  based solely on the angle of attack and the body's shape, disregarding Mach and Reynolds numbers. An augmented linear wing theory, combined with Newtonian impact theory (valid for  $\alpha < 10$ ), accounts for the influence of aerodynamic surfaces (fins) on  $C_N$  [6]. A model suggested in [7] has been applied in the normal force computation. (see equations in Appendix [5.3]).

The total normal coefficient is obtained:

$$(C_N)_{tot} = (C_N)_{body} + (C_N)_{fins1} + (C_N)_{fins2} \quad (3.3)$$

And the normal force :

$$N = q S_{ref} (C_N)_{tot} \quad (3.4)$$

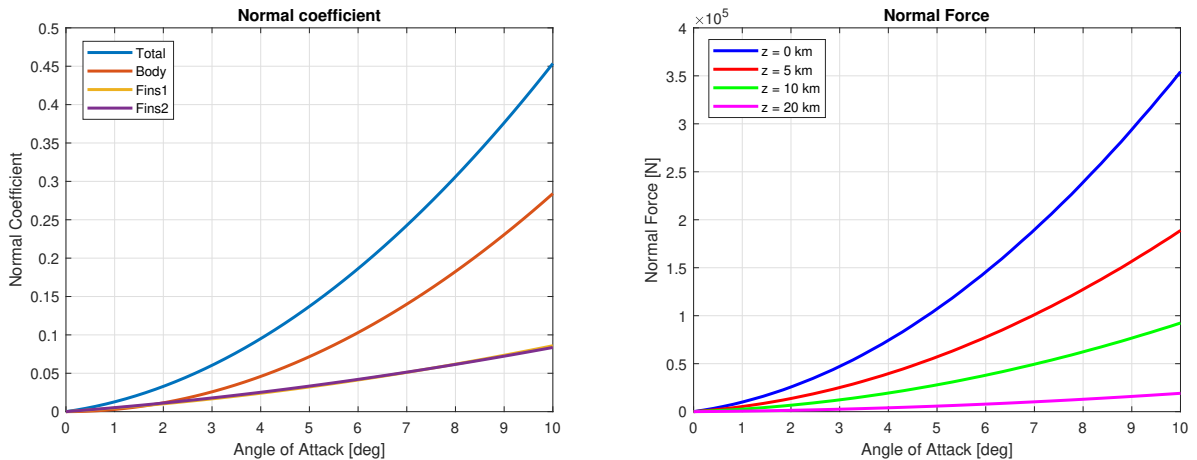


Figure 3.3: Normal coefficient and force dependence on  $\alpha$  and altitude at  $M = 2$

### 3.3.3 Re-entry

The dominant aerodynamic force during reentry is drag. In the case of symmetrical vehicles with a high flight path angle during atmospheric entry, the lift force is smaller than the drag force as shown in Figure 3.4 . The Knudsen Number ( $Kn$ ) serves as a measure for the spacing between molecules and is expressed :

$$Kn = \frac{\lambda}{L}$$

with  $\lambda$  = mean free path and  $L$  = representative physical length scale.

The reentry process can be classified into three regimes:

- Free Molecular flow :  $Kn > 10$
- Transition regime :  $0.001 - 0.01 < Kn < 10$
- Hypersonic continuum flow :  $Kn < 0.001 - 0.01$

Depending on the specific regime, the drag coefficient can be calculated using various formulas.  $C_d$  in free molecular flow regime is generally considered constant while in continuum flow regime is computed integrating the pressure distribution obtained with the modified Newton theory (see Appendix 5.3). One of advantage of the Paneling method is that aerodynamic forces can be locally computed on each panel. The paneling method demonstrates efficacy in the Hypersonic regime ( $M > 2$ ), specifically for dissociated flow. At lower Mach numbers, the hypothesis formulated by Newton become less significant. The model consider a cone shape. To enhance simplicity (as shown in the Appendix 5.3), the cone is represented schematically, with the incoming flux impacting only the base cone surface.

Figure in Appendix 5.5 illustrates the calculation of the pressure coefficient  $C_p$  for both Newton and modified Newton method. The  $C_p$  is obtained by integrating the pressure contribution over the surface. In Figure 3.4, it is observed that the drag increases with the Mach number as the flat plate surface is impacted by the flow. This behaviour can be explained physically by the absence of flow recirculation attached at the boundary layer. The altitude at which continuum flow dominates depends on the characteristic length  $L$ , with larger vehicles experiencing continuum flow at higher altitudes. The  $\alpha$  indicated in Figure 3.4 is referred as the angle between the i-direction and the incoming flux (see Appendix 5.3).

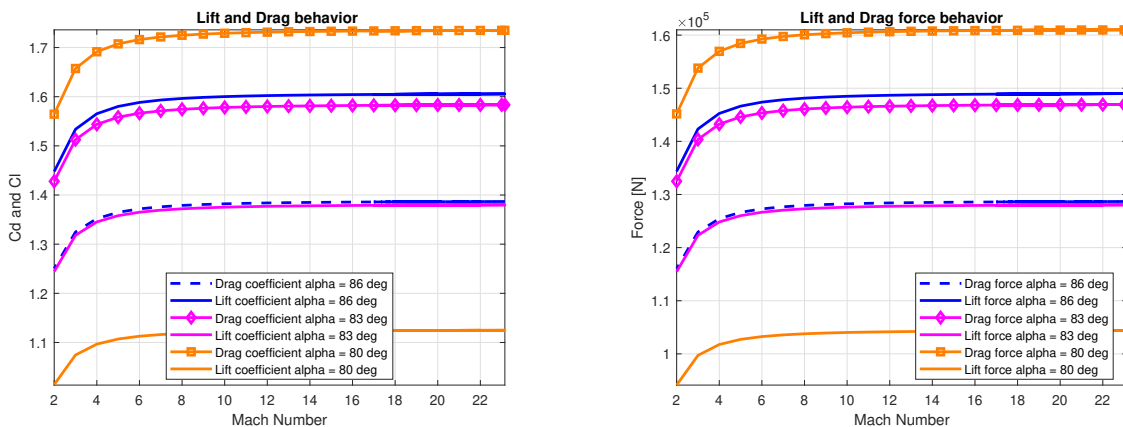


Figure 3.4: Drag and Lift coefficients and force dependence during reentry

The normal force and the normal coefficient are shown in Figure 3.5. The magnitude of  $F_n$  experienced in re-entry has the same order of magnitude of the ascent phase as shown

in Section 3.3.2. The normal forces should be higher as defined in [8]. This decrement can be given by a series of assumption made to implement this method : a calorically perfect non-reacting gas with the ratio of specific heats  $\gamma = 1.4$  is considered. The proper inclusion of chemically reacting effects is crucial for calculating an accurate shock-layer temperature; the assumption that  $\gamma$  is constant and equal to 1.4 is no longer valid when the gas temperature is increased to high values because the gas behaves as “non-ideal”. High-temperature chemically reacting flows can have an influence on lift, drag, and moments on a hypersonic vehicle.

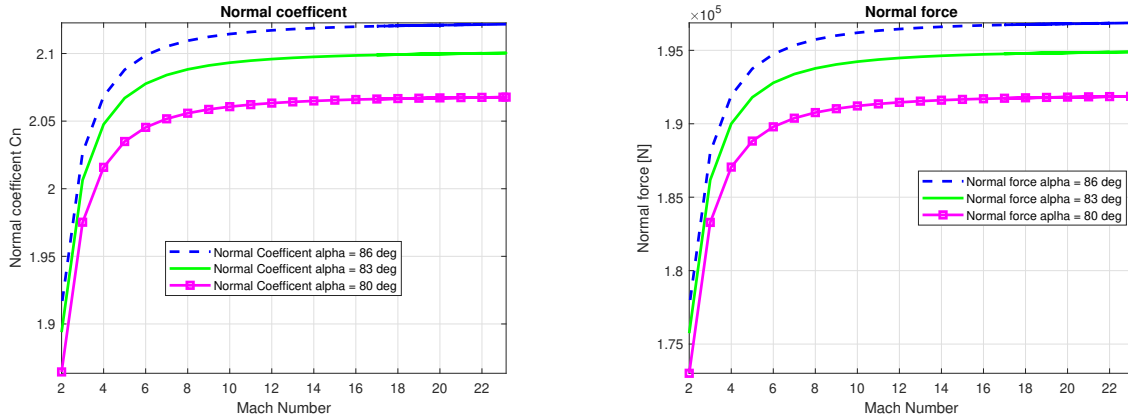


Figure 3.5: Normal coefficient and force dependence during reentry

Figure 3.6 depicts the variation of drag and lift coefficients ( $C_d$  and  $C_L$ ) along the altitude path. The decrease in drag is attributed to a reduction in velocity, a measure taken to safely reach the landing site without risking material damage, as elaborated in the Structure Reentry Section 3.4.1. At extremely low densities, the free molecular flow regime is present, where only a few molecules impact the surface per unit time and interactions are minimal. The full range of low-density effects is encountered by a hypersonic vehicle entering the atmosphere from space, down to an altitude where continuum aerodynamics takes over. The flow immediately at the leading edge is governed by low-density effects as shown in Figure 3.7 where initially a low  $C_d$  is experienced. This contribution is often ignored in practical aerodynamics, it becomes important for high-altitude hypersonic vehicles as the mission considered.

Figure 3.6 illustrates the variation of drag  $C_d$  and lift  $C_L$  along the altitude path. The decrease in drag is attributed to a reduction in velocity, a precautionary measure taken to ensure a safe landing without risking material damage, as detailed in Section 3.4.1.

At extremely low densities, the free molecular flow regime is prevalent, where only a few molecules impact the surface per unit time, and interactions are minimal. A hypersonic vehicle entering the atmosphere from space encounters the full range of low-density effects, down to an altitude where continuum aerodynamics takes over. The flow immediately at the leading edge is governed by low-density effects, as shown in Figure 3.7, where initially a low  $C_d$  is experienced. While this contribution is often disregarded in practical aerodynamics, it becomes crucial for high-altitude hypersonic vehicles, as considered in the mission.

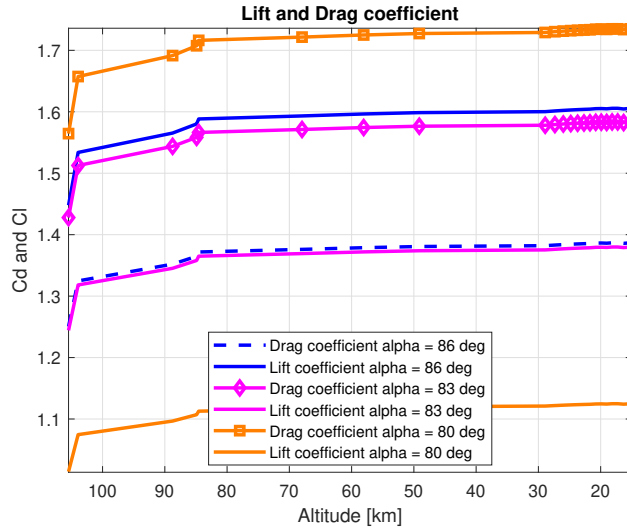


Figure 3.6: Lift and Drag coefficient ascent phase

In Figure 3.7, the variation of the drag coefficient  $C_d$  along the trajectory path is depicted. A low Knudsen number ( $Kn$ ) indicates that molecules are widely dispersed, resulting in fewer impacts and, consequently, a reduction in the drag coefficient  $C_d$ . Conversely, as the capsule enters the atmosphere, it undergoes a transition to a Hypersonic continuum flow, leading to an increase in drag until it reaches a constant value.

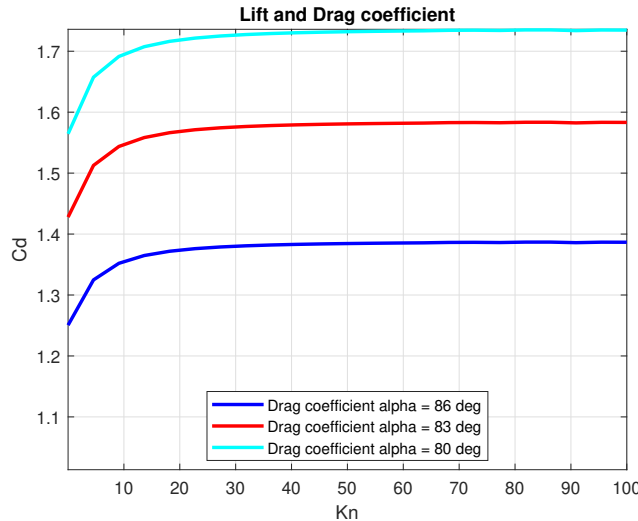


Figure 3.7: Drag coefficient vs Knudsen Number

### 3.3.4 Stability

#### Longitudinal Stability

The stability of the launcher is crucial in all missions as it directly impacts our trajectory. A launcher is considered stable when its center of pressure consistently remains below its center of gravity. This can be expressed:

$$x_{CG} \leq x_{CP} \quad (3.5)$$

Our launcher adheres to this condition passively for the first two stages. A control system is essential for the last stage and is implemented in Guidance part. Despite stability being ensured throughout the flight of the first two stages, it is necessary to integrate a control

system into our launcher for each stage ( see guidance part ). This is due to the requirement for a very precise trajectory for the landing of our capsule at a specific site.

The determination of the center of pressure and the center of gravity has been achieved through simulations conducted with OpenRocket, accounting for propellant consumption in the calculation of the center of gravity. OpenRocket performs aerodynamic analysis to establish the center of pressure, representing the position where aerodynamic forces are applied [9]. The analysis of longitudinal stability is conducted through the stability margin at each instant of the mission. We can see that, if the static stability margin is positive or equal, our launcher is stable, as shown 3.8

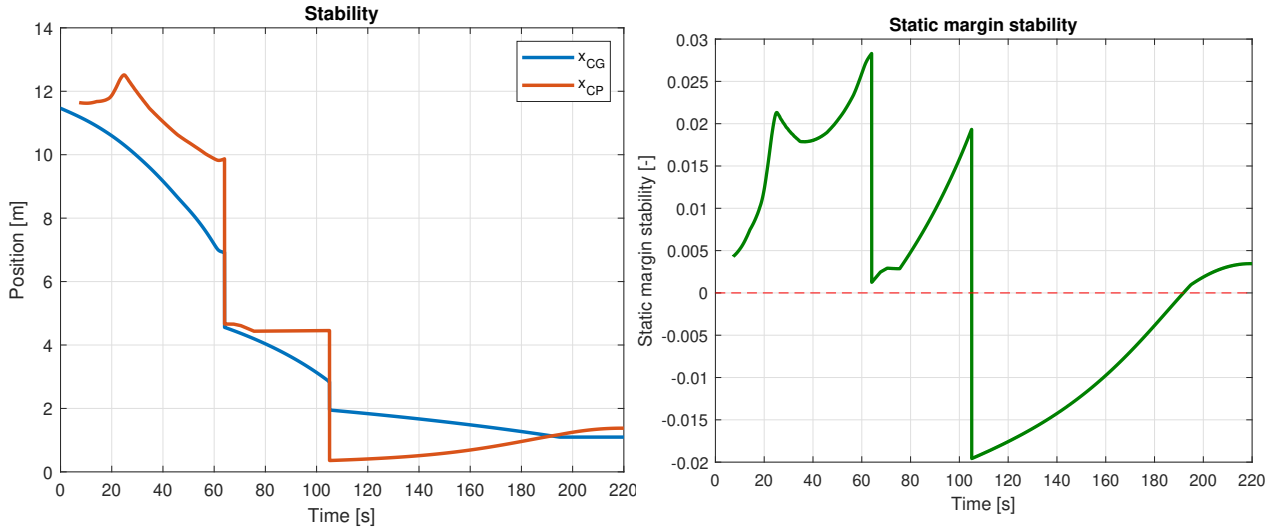


Figure 3.8: Center of gravity, center of pressure and static margin stability (distance from rocket tip) for a specific ballisitic trajectory

## Fins

Fins have two main objectives: they ensure stability for static flight stability or enable steering during motion. Our baseline does not have any fins. Fins have been designed for the first and second stages to improve the stability of our launcher by shifting downward its center of pressure. The choice to forego fins on the last stage of the rocket is driven by their benefits in scenarios involving high supersonic speeds and significant dynamic pressure. In this initial design, a boat-tail to diminish base drag has not been included, as it is not considered advantageous for a rocket that experiences a supersonic phase.

## 3.4 Structure Analysis

In this section will be discussed the structural aspect of the mission. The structure shall resist to all the forces and pressures that the body may encounter during the mission's lifetime (static and dynamic). In order to optimise the masses and the structural design of the mission, the values were changed together with the other parameters of the mission, until an acceptable error was reached (smaller than  $10^{-3}$ ). However as stated in the previous chapters, the angle of attack was not consider and it was assumed that the vehicle may interact three types of loads:

- **Axial Loads:** They were assumed to be equal to the sum of the thrust, drag forces and inertial forces, which were calculated at each instance of time during the ascending part of the mission. The results are shown in Figure 3.9. The thrust was considered to be constant during for each stage. The drag forces were calculated as function of

altitude and velocity, thus higher altitude, resulting in smaller drag forces. Lastly, for the calculation of inertial forces, it was considered the change in propellant mass for each stage.

- **Bending Loads:** The bending moments were considered to be produced by the normal forces, that were calculated at each instance using the Equation 5.3. By considering the mass evolution with time, the position of CG changes during flight, and thus also the distance between CG and CP. Thus the maximum value for bending moments it is reached during the first stage, before the detachment, when the surface area is maximum and also the length between the CP and CG for the first stack. An interesting behaviour occurs during the second stage when a local minimum is reached. In this region the variation of distance CG-CP has a more noticeable effect than that of Normal force.
- **Thermal Loads:** The thermal loads have a bigger impact on the capsule, thus this will be discussed more in details in 3.8.2. The structural aspect derived from the thermal loads was small enough that it could be neglected.

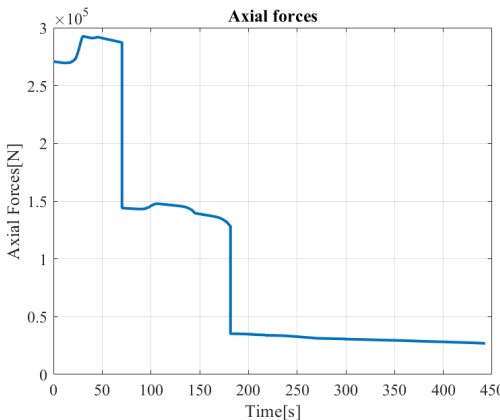


Figure 3.9: Axial Forces

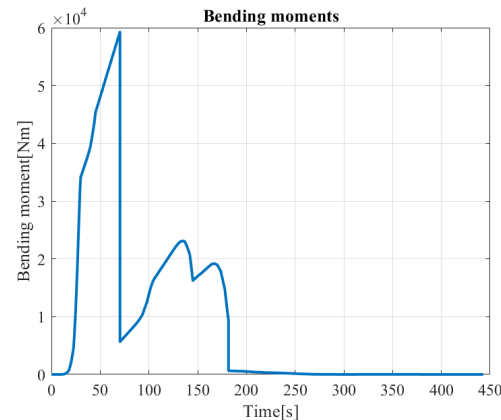


Figure 3.10: Maximum Bending Moments

## Materials

The structural analysis was continued with the selection of the materials. It is favorable to choose materials that meet the structural requirements, minimizing the mass and that are already in used in sector. Thus 10 materials were considered, and they were selected based on their structural properties. The final choice of the materials was made based on the resulted thickness and structural mass. From Table 3.2 it can be observed that the most suitable material would be Beryllium Alloy, as it would resist to buckling and axial forces, and the small density would help in reducing the overall mass of the structure. However, due to its toxic characteristics, it was not considered further, as it was not meeting the Ground Safety requirements. Magnesium Alloy has also been considered, but it is easily flammable and is not very resistant to corrosion, making it an unsuitable material. Composite materials, even though perform very good, the need of imposing a higher safety factors, decreases their advantages, in comparison with the metal alloys. Thus, the chosen material for the first and second stage was Aluminium Alloy 6061, regarding the structural components of the vehicle. For the third stage, the tanks material was considered to be Titanium Ti-6Al-4V, as this material performs better with smaller thicknesses (up to 4 mm). The analysis regarding the liquid tanks was used using the formulas in [10]. There were considered the thicknesses for the walls and for the domes, however, for safety reasons and manufacturing ease, it was continued with the larger thickness, even though this meant considering a higher inert mass.

Material	E[GPa]	$\sigma_y$ [MPa]	$\rho_{material}$ [ $\frac{kg}{m^3}$ ]	$T_{max-admiss}$ [C°]	$K[\frac{W}{mK}]$
<b>INCONEL X-750</b>	213.7	875.6	8280	1393	31.4
<b>Ti-6Al-4V</b>	113.8	970	4510	1604	7.5
<b>Carbon HM</b>	385	2000	1900	3650	1200
<b>S-Glass</b>	89	4600	2530	1725	1.35
<b>Kevlar</b>	131	2760	1455	500	0.04
<b>Steel</b>	205	1036	7850	1205	45
<b>Beryllium Alloy</b>	304	552	1827	1065	245
<b>Magnesium Alloy</b>	42	235	1827	400	50
<b>AS4C Carbon Epoxy</b>	231	4654	1780	300	0.25
<b>Aluminium Alloy 6061</b>	68.9	276	2700	582	152

Table 3.2: Considered Material

The material for the wings was considered to be AS4C Carbon Apoxy, which in this case even with a higher safety factor imposed, performed very well. The capsule material is INCONEL X-750. From a structural point of view, the differences between INCONEL and Aluminium 6061 were very small, but considering the thermal properties of these two materials, the former was chosen, primarily for its superior melting point.

### Mass Analysis

The mass estimation process began from calculating the structural mass of the each stage. The process began from the initial data of FLASH's baseline, afterwards the process being refines, and the obtained data integrated into the analysis. It was considered a safety factor of 1.3, as the materials considered were metals and the flight is unmanned. The body were considered to be composed of cylinders, thus the mass was calculated using the simplified formula of cylinder shell mass, while for the thickness, the following equations from [5] were used:

$$\begin{aligned} th_{BuckBend} &= 2.9r \frac{\sigma}{E} & th_{BuckAxial} &= 4.0r \frac{\sigma}{E} \\ th_{Thrust} &= \frac{T}{2\pi\sigma r} & th_{Pressure} &= \frac{pr}{\sigma} \\ th_{Gauge} &= 1.4r \left( \frac{7 \cdot 10^4 l^0}{E} \frac{l}{d} \right) .4 & th_{BendMoment} &= \frac{M}{\pi\sigma r^2} \end{aligned}$$

For the moments calculation, the load distribution term,  $c = 4$ , was considered to be for ejection load. The safety factor was applied directly to the overall thickness equation similar to: [5]

$$th = FOS \sqrt{th_{BuckBend}^2 + th_{BuckAxial}^2 + th_{Thrust}^2 + th_{Pressure}^2 + th_{Gauge}^2 + th_{BendMoment}^2} \quad (3.6)$$

where  $FOS$  represents the safety factor. The  $th/r$  ratio condition,  $0.003 < th/r < 0.03$ , is just satisfy by the aluminium.

The masses for the other components were calculating for each stage, the results and their equation being showed in Table 3.3.

#### 3.4.1 Structural Verification

Once all the data has been obtained, the thickness resulted from the loads was calculated and it should be smaller than the thickness obtained in the first step. For this step, the safety

Component	Formula	Total Mass[kg]
<b>Avionics</b>	$M_{av} = 10(M_0)^{0.361}$	321.06
<b>Wiring</b>	$M_{wiring} = 1.058L^{0.25}$	269.5
<b>Thurst Str.</b>	$M_{T-Struct} = 2.55 \cdot 10^{-4}T$	104.75
<b>Fins</b>	$M_{fins} = n_{fins}A_{fins}th_{fins}\rho_m$	109.82
<b>Engine Liquid</b>	$M_{Engine} = 7.81 \cdot 10^{-4}T + 3.37 \cdot 10^{-5}T\sqrt{\frac{A_e}{A_t}} + 59$	87
<b>Fairing</b>	$M_{fairing} = 4.95(A_{fairing})^{1.15}$	87
<b>Nozzle</b>	$M_{noz} = 0.256 \cdot 10^{-4} \left( \frac{(m_{prop}c^*)^{1.2}\epsilon^{0.3}}{p_c^{0.8}t_b^{0.6}(\tan(\theta_{cn})^{0.4})} \right)^{0.917}$	39.2
<b>Nose</b>	$M_{nose} = \rho_m th_{nose} S_{LateralNose}$	130.67

Table 3.3: Masses

factor was preserved. The capsule shall be strong enough to resist also to the landing impact. Thus, this situation was also considered, for the most difficult landing the capsule is designed to encounter. It was assumed that the most difficult land would be on the West-Coast, as the material of the landing surface would be sand. Compact sand was considered along with the conditions taken from the thermal analysis. The surface-impact-area was considered as a random function, that varies with the environmental factors, such as weather. There were simulated 1000 landings, and Figure 3.11 was obtained, which illustrates the thickness as a function of the impact area.

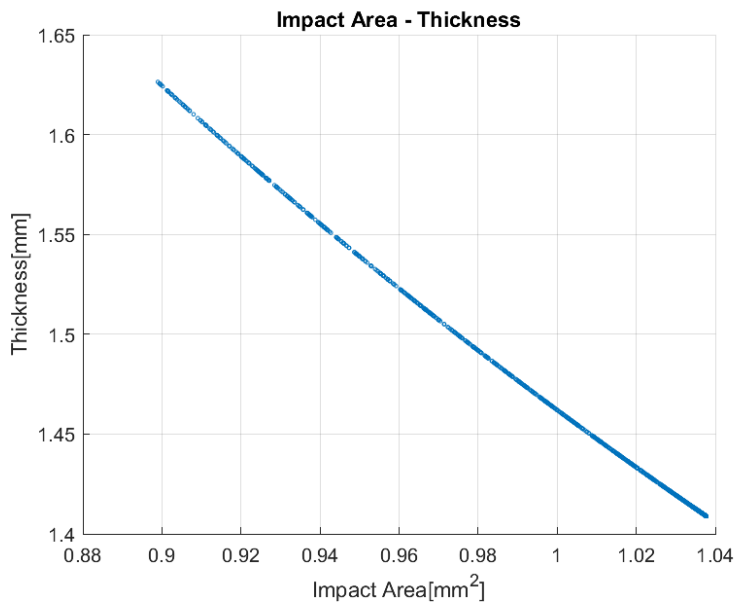


Figure 3.11: Impact Area

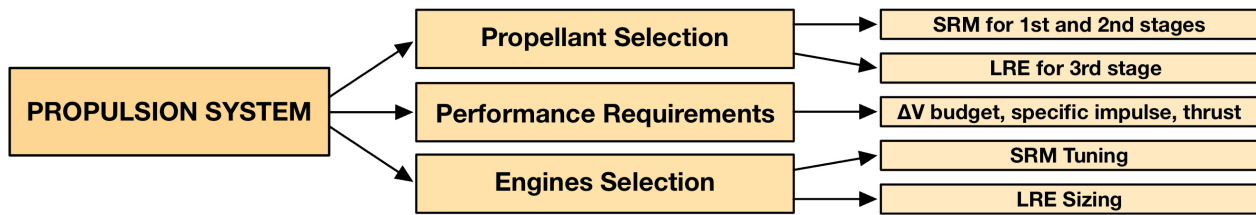


Figure 3.12: Propulsion system functional analysis

## 3.5 Propulsion

### Technology

The propulsion technology selection process is based on a series of criteria largely derived from customer requirements. Because of the strong dependence among ground systems (flight control, ground operations, maintenance) and flight systems (performances, flight control, operation of the rocket), several iteration processes are required in order to achieve the mission objectives [11]. The rocket has a 3 stage tandem configuration, which according to the baseline is the more suitable to deliver the required  $\Delta v$ . The first two stages are powered by solid fuel, while the third stage uses liquid propellant. The selection of solid propellant for the first 2 stages is based on the intrinsic advantages of this propulsion method. The primary benefits include its ease and speed of operation (in accordance with the readiness requirement), a high volumetric specific impulse (resulting in a compact system with reduced drag) and the ability to store the propellant under suitable conditions for 10-30 years. Due to high TRL and time-to-market customer requirements, the solid stages have been selected among the ones commercially available. Since the market is lacking in both solid motors and liquid engines capable of satisfying mission requirements for the third stage, a fitting liquid engine has been designed. In particular, by looking for available liquid engines, these turned out to be either toxic (large number of applications use hydrazine) or unable to match thrust requirements. As for the choice of a commercially accessible solid rocket motor, the main selection criteria were the dimensions and masses involved. Although a significant number of motors met the second criterion (with a necessary nozzle tuning), their geometry posed aerodynamic issues during flight (bodies too stubby).

### Engines Selection

Starting from the baseline performances and dimensions for each stage, a first rough selection has been made. This was then refined by verifying that the obtained configuration was able for the mission target to be achieved. The final assembly consists of:

- **CASTOR IV B [12] - First Stage:** this motor originally incorporates a regressive thrust-time trace for aerodynamic pressure considerations. Its employment in previous sounding rocket missions (e.g. MAXUS) as a first stage booster, together with proper dimensions and performances, made this motor a suitable choice for the assigned mission.
- **ORION 32 [12] - Second Stage:** nominally designed to be a second stage motor.
- **LIQUID ENGINE - Third Stage:** designed as reported in Section 3.5.2.

Table 3.4 shows the selected motors original specifications are shown, together with the required properties for the liquid engine.

	UNITS	CASTOR IV B	ORION 32	LRE
<b>Specific Impulse</b>	[s]	267.15	277.01	~300
<b>Thrust (Average)</b>	[kN]	423.30	128.11	~30
<b>Burning Time</b>	[s]	65	41	~100
<b>Total Length</b>	[m]	8.99	3.073	~2.5
<b>Diameter</b>	[m]	1.019	0.813	0.813
<b>Total Mass</b>	[kg]	11539.84	2141.41	TBD
<b>Propellant Mass</b>	[kg]	9974.50	1941.38	TBD
<b>Chamber Pressure (Average)</b>	[bar]	31.647	45.505	10
<b>Nozzle Exit Diameter</b>	[m]	0.902	0.632	~0.8
<b>Expansion Ratio</b>	[ $-$ ]	8	23	TBD
<b>O/F</b>	[ $-$ ]	Unknown	Unknown	~6

Table 3.4: SRM original and LRE expected properties.

### 3.5.1 Propellant

Starting from the baseline, due to the absence of information regarding the precise composition of the employed solid propellant (Hydroxyl-Terminated Polybutadiene (HTPB)), this has been modeled using typical values for civil applications (mass %):

- **HTPB:** 12%
- **Aluminum:** 16%
- **Ammonium Perchlorate:** 70%

For completeness, a small percentage of this model was subsequently employed to estimate the ratio between actual performance (derived from data sheets) and ideal performance (derived from Chemical Equilibrium Applications (CEA) software), particularly the specific impulse efficiency.

The same propellant model was then utilized to assess the real performance of the final propulsion system (first 2 stages), as both selected solid motors also employ HTPB (whose exact composition is unknown). For the third stage (LRE), a combination of  $H_2O_2$  (concentrated at 98%) as the oxidizer and RP-1 as the fuel has been adopted. This constitutes an environmentally friendly and fully storable combination, ensuring a high standard of safety during ground operations compared to cryogenic liquid propellants (although some precautions are still warranted with  $H_2O_2$ , given its corrosive nature at high concentrations).

### 3.5.2 Motor Modification and Design

#### SRM Modification

To adapt the first stage to meet the maximum acceleration requirements of the assigned mission while maintaining a high TRL, only nozzle modifications were implemented. Specifically, a change in shape from conical to bell-shaped and an increase in the throat area were performed, keeping all other parameters unchanged. This results in a decrease in the combustion chamber pressure, consequently leading to a reduction in the burning rate, an increase in the combustion time, and a decrease in thrust. The modified engine achieves an approximate constant thrust profile, which does not pose issues in terms of maximum acceleration and dynamic pressure, as these were the parameters upon which the modification was based. Table 3.5 lists the first stage engine parameters following the modification, while the Appendix 5.9 includes a comparison between the original and the modified nozzle. As for the second stage engine, no modifications were made since the parameters of the original engine were already suitable for the assigned mission profile.

	UNITS	CASTOR IV B	ORION 32	LRE
<b>Specific Impulse</b>	[s]	243.50	277.01	317.7
<b>Thrust (average)</b>	[kN]	138.64	128.11	47.68
<b>Burning Time</b>	[s]	70.3	41	150
<b>Total Length</b>	[m]	8.99	3.073	6.045
<b>Diameter</b>	[m]	1.040	0.835	0.835
<b>Total Mass</b>	[kg]	11539.84	2141.41	3104.5
<b>Propellant Mass</b>	[kg]	9974.50	1941.38	2284.7
<b>Chamber Pressure (average)</b>	[bar]	22.85	45.505	10
<b>Nozzle Exit Diameter</b>	[m]	0.854	0.632	0.8
<b>Expansion Ratio</b>	[ $-$ ]	5.9	23	17.7
<b>O/F</b>	[ $-$ ]	Unknown	Unknown	6.11

Table 3.5: Tuned solid boosters parameters and final LRE design parameters. The SRM diameters are different due to the inclusion and/or modification of structural components.

#### LRE Design

The design guidelines for the sizing of the liquid third stage were introduced in Section 3.5.1. Starting from the selected propellant couple and conducting a simulation using NASA CEA code, the optimal mixture ratio was determined. Subsequently, with this information, along with the relative densities of the oxidizer and fuel and the desired combustion chamber pressure, the sizing of the tanks was carried out. In order to create a compact system, a shared-bulkhead configuration was chosen for the propellant tanks (see Appendix 5.10) and an elastomeric diaphragm has been used in each tank to reduce sloshing phenomena. Since

the third stage is powered by a pressurized system, sizing of the pressurizing gas tank was also necessary. In tanks sizing, pressure losses induced by real phenomena (8%) were taken into account. For the sizing of the combustion chamber, the characteristic length value for the  $H_2O_2$  - RP-1 propellant couple was used: this already included the presence of a catalytic bed for  $H_2O_2$  decomposition, which, however, was not considered in the final sizing as it is a preliminary design. Furthermore, for completeness, the selection and sizing of an injector plate suitable for the chosen propellant couple and the desired Oxidizer-to-Fuel (O/F) ratio would be necessary. The large quantity of oxidizer compared to fuel, coupled with the dissociated state at which the  $H_2O_2$  injection occurs in the combustion chamber, justifies the choice of an injection plate with a concentric tube configuration, where the dissociated  $H_2O_2$  passes through the outer duct. Subsequently, the nozzle was designed as a bell-shaped Rao nozzle: in this design, the contraction ratio was assumed as a typical value, while the expansion ratio was used as a variable. To make the compatibility with the required  $\Delta v$  more flexible, at least in a preliminary phase, the burning time was also considered as a variable.

### 3.5.3 Stage Separation Systems

During the stage separation, some main requirements needs to be fulfilled [13]:

- the zero-control phase duration of the flight has to be very low, so separation needs to occur in minimum time;
- the shock caused by separation must not affect the feasibility of the mission, that is minimum transmission of the perturbation and no damage due to debris contamination to the continuing stage;
- the structural integrity among two attached bodies has to be maintained, in order to guarantee the joint to withstand the dynamic loads encountered during the flight.

In addition, high TRL requirement led to stage separation mechanisms such as collet mechanism and Flexible Linear Shaped Charges (FLSC), which are used in both Geosynchronous Satellite Launch Vehicle (GSLV) and Polar Satellite Launch Vehicle (PSLV). Ring-shaped charges positioned at the stage interfaces will ensure both the separation of the expended stage and the relative inter-stage, which in turn will be severed by using linearly shaped charges located on the internal wall. For each inter-stage, this system will be composed of two ring-shaped charges and four linearly shaped charges (for redundancy concerns), which will be simultaneously triggered by means of an electrical signal. This solution is very simple and guarantees structural continuity before being activated, but it generates pretty high levels of shock and contamination, depending on the thickness of the kind of material being cut. The capsule separation occurs by severing the interface, that is a collet mechanism: this is a low shock, fast response ( $\tilde{20}\text{ms}$ ) and debris-free solution which still allows to carry high structural loads. Also in this case the separation occurs by means of pyro charges, which are ignited in order to activate the collet release mechanism.

### Flight Termination System

For safety reasons, the launch vehicle must be equipped with a flight termination system (Flight Termination System (FTS)) in case the capability of controlling the flight is inadmissible. Its purpose is to destroy the components for ensuring ground safety, during the different phases of the flight. As the chosen vehicle is a 3-stage vehicle, each of the stages must be equipped with its own FTS. In the case of solid-fuel vehicle, the FTS engender cuts into the propellant and its casing, breaking the entire vehicle into small pieces. The FTS is done through Linear Shaped Charge (LSC), placed along the rocket. The house shape was chosen

because of its higher rigidity, making it more suitable for a FTS. The LSCs will be placed on both sides of the propellant casing, in the first 2 stages, between the propellant casing and the outer housing, similar to [14]. The explosive must be strong enough to penetrate through the solid propellant and reach the bore. The LSCs will be placed along the propellant casing of each stage. For redundancy reasons each component of the flight termination system will be doubled to obtain a high level of reliability(to obtain a small margin of error). For the stage that uses liquid propellant the arm command is used to turn off any liquid engines of the vehicle. As an explosion of the propellant and of the oxidizer is undesired, the LSCs will be placed on the top part of each tank. It was assumed that at the moment of FTS activation a certain quantity of fuel will be burnt. For redundancy reasons, as a very low level of error is allowed, each system's device will be doubled. Thus there will be two sets of batteries, receivers, transmitters, tracking system and sets of LSCs, for all stages. [15][16]

## 3.6 Trajectory

### 3.6.1 Models

In order to accurately simulate a long range trajectory such as the one required by the customer, a round-Earth model must be implemented. In this model, the dynamics of the rocket are described by the following equations:

$$\begin{cases} \dot{r} = v \sin \gamma \\ \dot{v} = \frac{T}{m} - g \sin \gamma - \frac{D}{m} \\ \dot{\omega} = \frac{v}{r} \cos \gamma \\ \dot{\gamma} = \left( \frac{v}{r} - \frac{g}{v} \right) \cos \gamma \\ \dot{m} = -\frac{T_0}{I_S g_0} \end{cases} \quad (3.7)$$

Where

$$\begin{cases} T = T_0 + (P_e - P_{atm}) A_e \\ g = g_0 \left( \frac{R_E}{r} \right)^2 \end{cases} \quad (3.8)$$

For the first two stages, which use SRMs,  $T_0$  was assumed to be constant and equal to the mean thrust. This is, of course, an approximation that does not take into account the internal ballistics of the SRMs. In the third stage's case,  $T_0$  was also assumed to be constant, so no throttling of the LRE is considered. These equations are valid for all flight phases, with parameters such as  $A_{ref}$ ,  $C_D$ ,  $m_0$ , etc changing according to the stage being fired at any point in time. Additionally, normal aerodynamic forces are assumed to be zero because this is a best case scenario, in which the angle of attack is always zero.

### 3.6.2 Implementation

A constrained optimization algorithm was implemented in order to minimize the time of flight while respecting design constraints and client requirements. The constrained optimization problem is defined as follows:

$$\min_{h_{gt}, \gamma_0, t_{b,3}, \Delta\gamma_{0,3}} t_{land} \quad \text{subject to} \quad \begin{cases} \max(q) \leq 70 \text{ kPa} \\ \max(\dot{v}) \leq 9 \cdot g_0 \\ \omega(t_{land}) = \cos^{-1}\left(\frac{\mathbf{r}_0 \cdot \mathbf{r}_f(t_{land})}{R_E^2}\right) \\ r(t_{land}) = R_E \end{cases} \quad (3.9)$$

This algorithm includes the drag coefficient as a function of the Mach number, the 1976 U.S Standard Atmosphere [4], the opening of the drogue and main parachutes with their filling times and the change of the rocket's mass and thrust according to the stage being fired. However, it does not include any control logic, with the maximum downrange distance being determined by  $h_{gt}$ ,  $\gamma_0$ ,  $t_{b,3}$ , and  $\Delta\gamma_{0,3}$ .

### 3.6.3 Nominal trajectory simulation

After performing the optimization for each of the landing sites, the results shown in Table 3.6 were obtained.

	<b>West Coast</b>	<b>Midwest</b>	<b>East Coast</b>
$h_{gt}$ [km]	10	0.113	1.553
$\gamma_0$ [deg]	45	89.445	69.811
$t_{b,3}$ [s]	150	150	150
$\Delta\gamma_{0,3}$ [deg]	8.3698	-54.655	2.1217
$t_{land}$ [min]	31.8425	28.0408	29.1489
<b>Downrange distance [km]</b>	<b>6932.9</b>	<b>5361.1</b>	<b>6002.1</b>

Table 3.6: Optimization results

Having obtained these results, the nominal trajectories were computed. The time history of the dynamic pressure, Mach number, Altitude and Acceleration for both the ascent and descent phases several important parameters for the ascent and descent phases, for every landing site, can be found in Appendix 5.7, along with the Altitude vs Downrange plot.

### 3.6.4 Monte Carlo analysis

For each of the three trajectories, a Montecarlo analysis on the rocket range has been conducted, incorporating perturbations in the initial state. The initial state was perturbed by considering a Gaussian distribution for each variable, with a standard deviation of  $\pm 1\%$  of the nominal value. A total of 5000 samples were generated for each arrival site. It is crucial to note that wind, usually a significant source of uncertainty in trajectory analysis, has not been considered in this preliminary phase. For each of the cases the mean and the standard deviation of the range has been computed.

	Mean [km]	STD [km]
<b>East</b>	4956,96	1148,43
<b>Midwest</b>	2300,03	1457,18
<b>West</b>	2352,89	1450,66

Table 3.7: Montecarlo Analysis on the Range

The Montecarlo analysis demonstrates that with an increasing number of samples, the range converges towards the nominal range, indicating minimal errors in the landing. However the standard deviation appears to be very high making the control of the rocket an important part of the mission. This trend is illustrated in Figure 3.13 for the West landing site. Similar analyses were conducted for the other landing sites as shown in Figure 5.23 and Figure 5.24

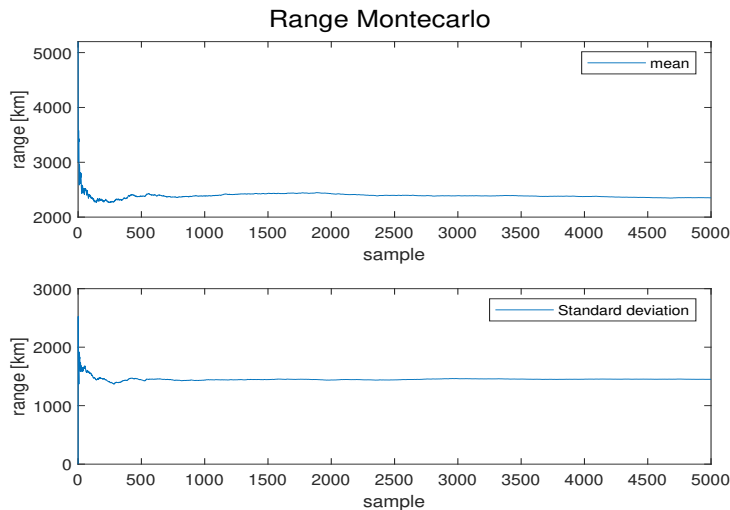


Figure 3.13: Montecarlo analysis for West landing site

The same analytical approach applied to the impact point analysis can also be employed to ensure the safe disposal of each stage. This methodology allows us to ascertain that the stages will descend in locations where they pose no harm to individuals or property, thereby ensuring a safe disposal process.

## 3.7 Guidance

Upon the implementation of all other aspects of the mission, the Guidance, Navigation and Control (GNC) system is considered. This is essential as a mapping of the state of the launch vehicle is required at each moment to ascertain whether any corrective maneuvers are necessary to remain on the nominal trajectory. The foremost requirement of this subsystem deals with the stability of the vehicle. Specifically, with the GNC system, it is important to ensure continuous stability of the system. For this mission, an inertial control without terminal guidance is under consideration. Specifically, Flash is categorized as a non-homing inertially guided vehicle. A simplified GNC system is implemented for each of the three calculated nominal trajectories. In the case of each stage, a Thrust Vector Control (TVC) strategy is employed and governed by a Proportional-Integral-Derivative (PID) controller, while for the capsule the control is performed by the use of actuators. Notably, a Shallow

Throttling method, allowing for an increase of up to +10% of the nominal thrust [9], is utilized to manage the lateral deviation of the rocket. The control angle, denoted as  $\delta$ , is computed using a PID law expressed as  $\delta = -k_1\theta - k_2\dot{\theta} - k_3\alpha$ . The details of this PID controller are outlined in Table 3.8. The computed  $\delta$  is then employed to update the state vector, as described in Appendix [5.9].

$k_1$	$k_2$	$k_3$
2	0.8	3.164

Table 3.8: PID law

It is observed that in the first stage, where no control is required, the  $\delta$  angle remains consistently equal to zero, as does the angle of attack. From the second stage, when the TVC system becomes active, slight variations in all angles are noticeable. The controlled system ensures that the lateral deviation remains consistently minimal. Consequently, the rocket remains in close proximity to the nominal trajectory throughout the mission.

## 3.8 Atmospheric re-entry and landing

### 3.8.1 Parachutes sizing

#### Preliminary considerations

The recovery analysis aims to design a set of parachutes able to carry the payload back to the ground with an imposed touchdown velocity set to  $7m/s$ . Starting from the altitude at which the drogue parachute is able to work safely, first the drogue and then the main parachute are opened to slow down the payload descent until the target landing velocity and keeping the shocks bearable for the payload. The first parachute is a supersonic drag parachute whose role is to slow down the payload at high altitude and high velocity; it has a smaller surface than the main one since at high altitudes air is rarefied and a high surface parachute would take a long time to fill up or could even fail to open completely. Indeed, the longer the filling time of the parachute, the longer the time in which the payload accelerates instead of slowing down: until the parachute is not completely open it cannot counteract the payload inertia. The main parachute has a bigger surface area than the drogue and its aim is to decelerate the payload to the final touchdown velocity.

#### Design

The sizing of parachutes starts from the mass of the payload  $m_{pay}$  and the imposed touchdown velocity  $v$ . Accordingly to [17], ringsail parachutes are commonly used for subsonic recoveries that require a low landing speed, plus they are easy to be manufactured. For drogue parachutes that require stabilization and deceleration at supersonic speeds, the choice can fall to a hemispherical ribbon chute. From Figure 5.19 the value of  $C_D$ , and  $C_L$ , for the drogue and main parachute are fixed considering the type and shape chosen. The design begins with the sizing of the main parachute surface imposing the equilibrium between the weight of the payload and the drag force given by the parachute at touchdown as:

$$D = \frac{1}{2}\rho v^2 A_{ref} C_D = m_{pay}g \quad (3.10)$$

where the only unknown is the main parachute surface, hence :

$$A_{ref} = \frac{2m_{pay}g}{\rho v^2 C_D} \quad (3.11)$$

For the main,  $\rho$  is computed at the ground and  $v$  is the landing velocity. For what concerns the drogue chute, a typical rule of thumb [18] is considered, taking  $S_{drogue}$  as a fraction of  $S_{main}$ .

From Figure 5.20, the mass of the two parachutes is retrieved, knowing their diameters: the final results are summarized in Table 3.9.

	<b>Surface</b> [ $m^2$ ]	<b>Diameter</b> [m]	<b>Mass</b> [kg]	$C_D$ [-]	$C_X$ [-]
<b>Drogue</b>	8.09	3.21	2.00	0.8	1.1
<b>Main</b>	134.87	13.10	8.00	0.4	1.15

Table 3.9: Drogue and main parachutes data

## Opening altitude and shocks evaluation

Proceeding with the design, the remaining variable is the opening altitude of the parachutes. These altitudes are chosen considering both the operating speed condition and the filling times. According to Planz's method described in [19], the shock evaluation is performed starting from the opening force:

$$F = \frac{1}{2}\rho v^2 S C_X X \quad (3.12)$$

where  $v$  and  $\rho$  are chosen to fulfill the previous considerations and  $X$  is the force reduction parameter that can be computed from the Figure 5.22 knowing the ballistic parameter  $A$ . For each altitude the velocity  $v$ , the filling time  $t_{fill}$  and the ballistic coefficient  $A$  are computed:

$$v(z) = \sqrt{\frac{2m_{pay}g}{C_D S \rho(z)}} \quad t_{fill} = \frac{nd}{v(z)} \quad A = \frac{2m_{pay}}{S \rho(z) t_{fill} v(z)} \quad (3.13)$$

where  $n$  is the canopy fill constant retrieved from Figure 5.21. Finally the shock can be computed as:

$$a = \frac{F}{m_{pay}g} \quad (3.14)$$

	<b>Opening altitude</b> [km]	<b>v</b> [ $\frac{m}{s}$ ]	$t_{fill}$ [s]	<b>X</b> [-]	<b>a</b> [g]
<b>Drogue</b>	16.31	1029	0.19	1	2.875
<b>Main</b>	12.25	51.45	9.24	0.2	0.275

Table 3.10: Recovery results

The shocks obtained with the previous recovery sequence can be sustained by the payload without damaging it.

### 3.8.2 Thermal analysis

During the mission, the heating due to air flowing along the rocket's surface could cause general structural failures with catastrophic consequences, given the high velocities reached especially during re-entry. For this reason, a Thermal Protection System (TPS) is needed. The energy balance equation for the general heat transfer problem has been derived:

$$\rho_m c V \frac{\partial T}{\partial t} = \dot{q}_{tot} A - \epsilon \sigma A T^4 \quad (3.15)$$

where  $T$  is the material's temperature,  $V$  and  $A$  are the volume and the area of the thermal protection material,  $c$  is the heat capacity coefficient and  $\sigma$  is the Stefan-Boltzmann constant.

Another important source of stress is aerodynamic heating  $\dot{q}_{tot}$ , computed following [7]:

$$\dot{q}_{tot} = A_{nose} (C \rho_{(z)}^{0.5} v_{(z)}^3) \quad (3.16)$$

where  $C = 1.7415 \cdot 10^{-4} / R_n$  with  $R_n$  the curvature of the thermal shield,  $v(z)$  and  $\rho(z)$  are respectively the velocity and the density at the altitude  $z$ . It is important to highlight that the TPS materials which will be applied to protect the surfaces do not have any structural function.

### Nose thermal protection

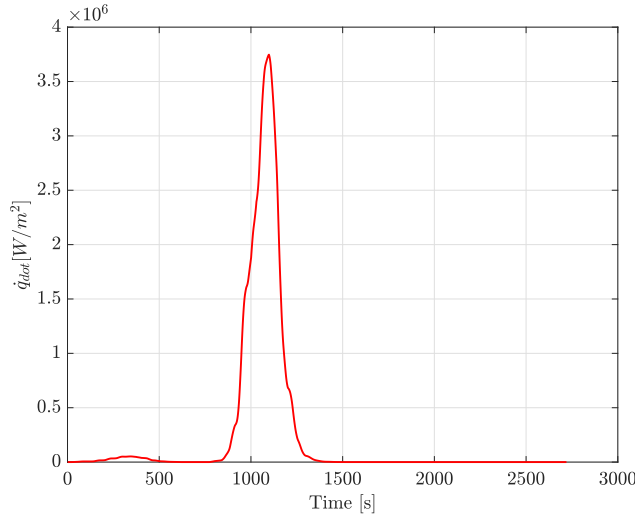
The nose plays a critical part in modifying the flux of air surrounding the launcher, hence it is desirable that neither its geometrical characteristics nor its structural integrity change over time. Inconel X was selected as material for the capsule.

From equations 3.15 and 3.16 is possible to retrieve the capsule mass and so the total thickness needed to withstand the load. The thickness value  $th_{capsule} = 5mm$  also considers manufacturing-related issues and it is increased until the final temperature is minor than 80% of the melting one.

$$m_{capsule} = \frac{1}{c T} \int_0^{t_f} \dot{q}_{tot} dt \quad (3.17)$$

### Re-entry thermal protection system

For the re-entry phase, given the high speeds involved, an ablative heat shield was chosen. The temperature behaviour on the front face of the capsule have been found as a function of the trajectory, by integrating 3.15 from the apogee to the end of the mission. Looking at Figure 3.14 the peak of heat flux occurs in the re-entry phase.

Figure 3.14:  $\dot{q}_{tot}$  over time

Following this result, three different materials have been selected: Teflon, MA-25S, and Phenolic Nylon. Their properties are summarized in Table 3.11

Materials	$\rho_m$ [ $\frac{kg}{m^3}$ ]	$c$ [ $\frac{J}{kgK}$ ]	$T_{abl}[K]$	$\epsilon$ [-]	$Q_{abl}$ [ $\frac{J}{kg}$ ]	$\xi_{abl}$ [mm]	$m_{abl}$ [kg]
<b>Teflon</b>	2162	1674	833	0.38	7257120	25.00	28.07
<b>MA-25S</b>	400	1256	783	0.8	55791436	19.20	3.98
<b>Phenolyc Nylon</b>	1633	1151	1900	0.9	1040000	12.80	10.85

Table 3.11: Ablative material's properties and resulting thicknesses and masses

In order to assess the best material for the purpose of this mission, a trade-off between the ablative material consumed during the re-entry phase and heat shield's total mass was made.

The recession rate for the different materials has been computed as [20]:

$$v_{abl} = \frac{\dot{q}_{tot} - \sigma\epsilon T_{abl}^4}{\rho_m[c(T_{abl} - T_\infty(z) + Q_{abl}]} \quad (3.18)$$

where  $T_{abl}$  is the ablation temperature i.e. the temperature at which the material starts the ablative process,  $T_\infty(z)$  is the standard atmospheric temperature and  $Q_{abl}$  is the heat of ablation.

Therefore, by integrating  $v_{abl}$  the total consumed material was obtained. Finally, the MA-25S has been chosen as material for the thermal shield because of its smallest mass.

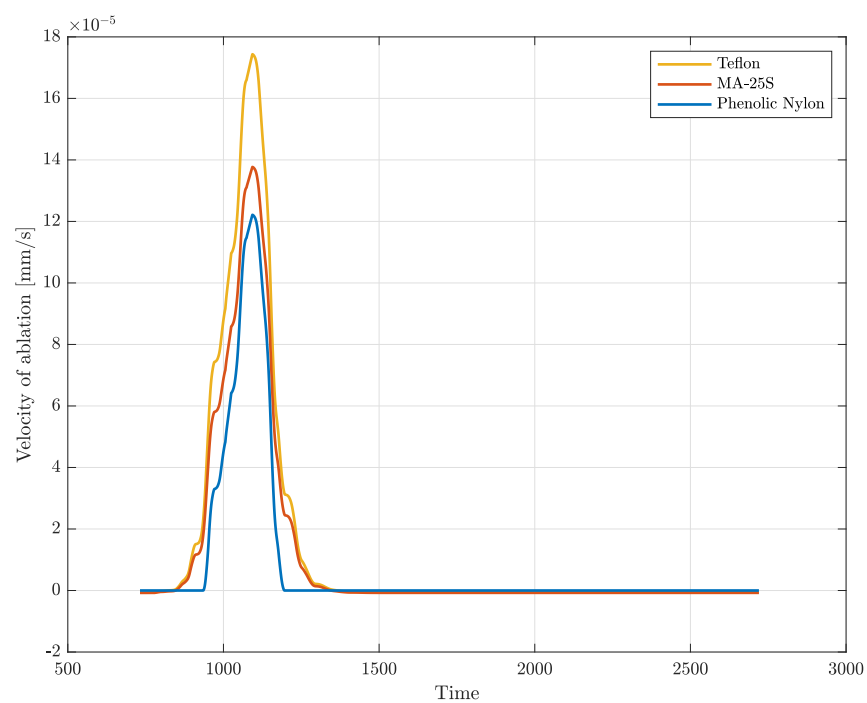


Figure 3.15: Ablation temperature over time

# Chapter 4

## TRL and Client Requirements

### 4.1 TRL and AD<sup>2</sup>

To meet the client's requirements, technologies with a high TRL were prioritized. Given the short time-to-market target of 5 years, developing overly complex or numerous new technologies is not feasible. Instead, we focus on leveraging existing technologies, making necessary modifications and improvements as needed.

	TRL <sub>START</sub>	TRL <sub>END</sub>	AD <sup>2</sup>
Engines	6	8	2
Materials	7	8	2
Fins	6	9	2
Capsule	6	8	2
Parachutes	6	9	2
Control System	4	9	3

Table 4.1: TRL table summary

#### 4.1.1 Engines

The choice of commercially available engines for the first two stages is advantageous from a Technology Readiness Level perspective, since there is no need to develop a new technology for the propellant, nor is there a need for a testing phase. In fact, the first stage has already completed missions (TRL = 9), while the second stage, although not yet utilized in any application, features all components already flight-tested (TRL = 8). The modifications made to the first stage lower the TRL, but the reduction is minimal since only the nozzle has been modified (TRL = 6). The decision to design a liquid stage is a technological drawback from a design viewpoint, although the selected propellant couple and technology have been extensively studied and flight-proven (TRL = 3).

#### 4.1.2 Materials

All the material considered have already been used in the past applications for structural reasons in the space industry. Even though some of them don't have a wide application in

structural design, the material chosen after the analysis have a long usage history, with much research being completed until this moment.(TRL - 9).[21] [22]

#### 4.1.3 Fins

The fins utilized in FLASH are derived from the OpenRocket iteration. Specifically, the fin shapes are chosen from [5], while the dimensions are optimized through iteration to reduce drag and enhance stability 5.6. Since the fins selected for FLASH are standard but have not yet undergone flight testing, a Technology Readiness Level (TRL) of 6 is assigned.

#### 4.1.4 Capsule

The chosen material is widely employed in the aerospace sector for high-temperature applications (TRL = 6), and the same considerations apply to both the heat shield's geometry and material (TRL = 6) and the capsule's shape, which has been derived from existing spacecrafts, but with different mission profiles (TRL = 6).

#### 4.1.5 Parachute

The parachute technology selected for the FLASH mission is a well-established standard. The chosen parachute material boasts a significant heritage in space applications [23]. Considering the proven track record of the technology, a Technology Readiness Level (TRL) of 6 is assigned.

#### 4.1.6 Control System

The chosen control system is theoretical, necessitating further research to fine-tune it appropriately. Therefore, the initial (TRL) is set at 4. As the rocket undergoes its inaugural launch, the TRL is expected to increase to the maximum value of 9, indicating its achievement of full operational capability.

### 4.2 Client requirements

In this section, the methods employed by Team Flash to ensure the fulfillment of customer requirements are discussed.

#### 4.2.1 Ready within hours

To meet this requirement, the team decided to shift its focus to a capsule instead of a fairing. The primary consideration in choosing the capsule is that in space applications, precision is often prioritized over velocity. In this case, to ensure precision and velocity, we have adopted a collect system. The collect system is based on the Crew Dragon system, ensuring both operational velocity for launch and a high TRL. This design decision strategically reduces the operational lead time preceding the initiation of the launch sequence. If FLASH will obtain the mission further development will be analyzed. A draft of the system is shown in the Appendix 5.5.

#### 4.2.2 Safety on ground

A detailed discussion is necessary for ground safety, as this requirement significantly influences propellant selection. The propellant used for the first two solid stages is not environmentally friendly, and while pollution is not dramatically expanded, Team FLASH requires an exclusion zone with a radius of 10 km to ensure safety. For the last liquid engine motor, higher attention needs to be paid. The propellant is classified as green, in accordance with [24], unless a strictly regulated rule, as outlined in [25], is required to manage liquid propellants.

# Chapter 5

## Conclusion

This report present the preliminary design process for an Intercontinental Suborbital Cargo Rocket, resulting in the development of a preliminary design for FLASH. The mission outcome effectively meets nearly all of the customer's requirements. However, certain challenges related to maximum axial acceleration have been identified. Consequently, further modifications are necessary, and discussions with the client are underway to ensure the successful conclusion of the mission. It should be noted that, during the descent phase, the accelerations imposed on the capsule by aerodynamic drag exceed the limit of  $9g$ . This is due to the extremely high dynamic pressure that the capsule experiences when it reaches the lower parts of the atmosphere. Slowing down the payload capsule in the upper atmosphere with different methods than aerodynamics would be beneficial and should be explored in further stages of the design process. The Table below provides details of the verifications conducted at the conclusion of the preliminary design phase:

Requirements	Fulfilment [Yes/No]
Landing range flexibility	Yes
Payload range 10 to 100 kg	Yes
Time-to-market 5 years	Yes
Maximum acceleration 9g	No
Safe disposal of stages	Yes
Safety on ground in case of accident	Yes

Table 5.1: Requirements Fulfilment

In conclusion, the presented report serves as a reasonable foundation for future studies and developments.

## 5.1 Project Management Appendix

### Mission concept synthesis

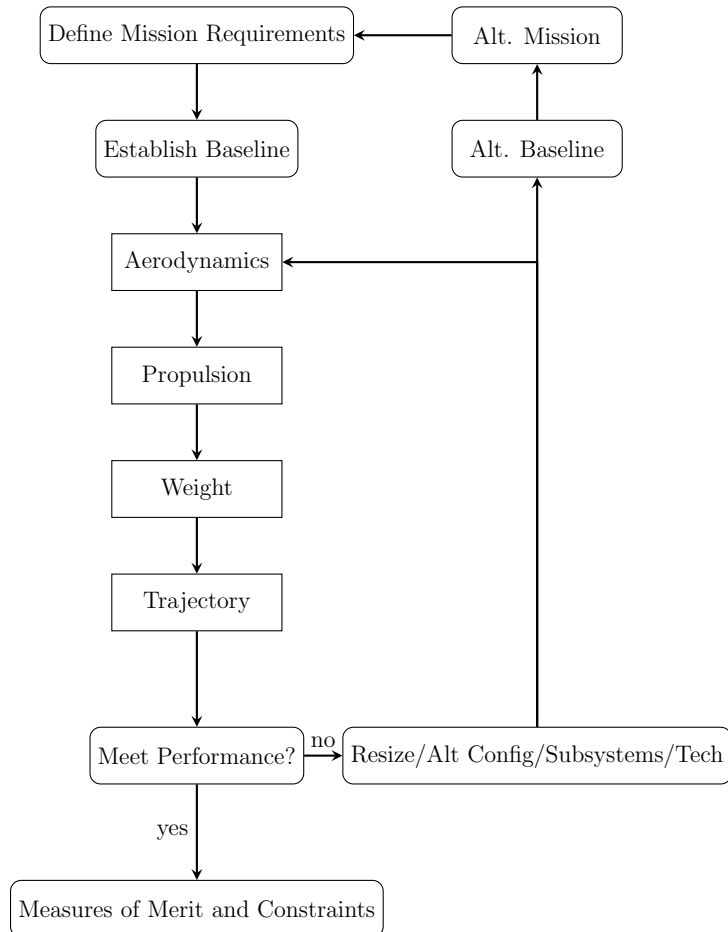


Figure 5.1: Mission concept synthesis requires evaluation of alternatives (alt.) and iterations, from [5]

## HoQ

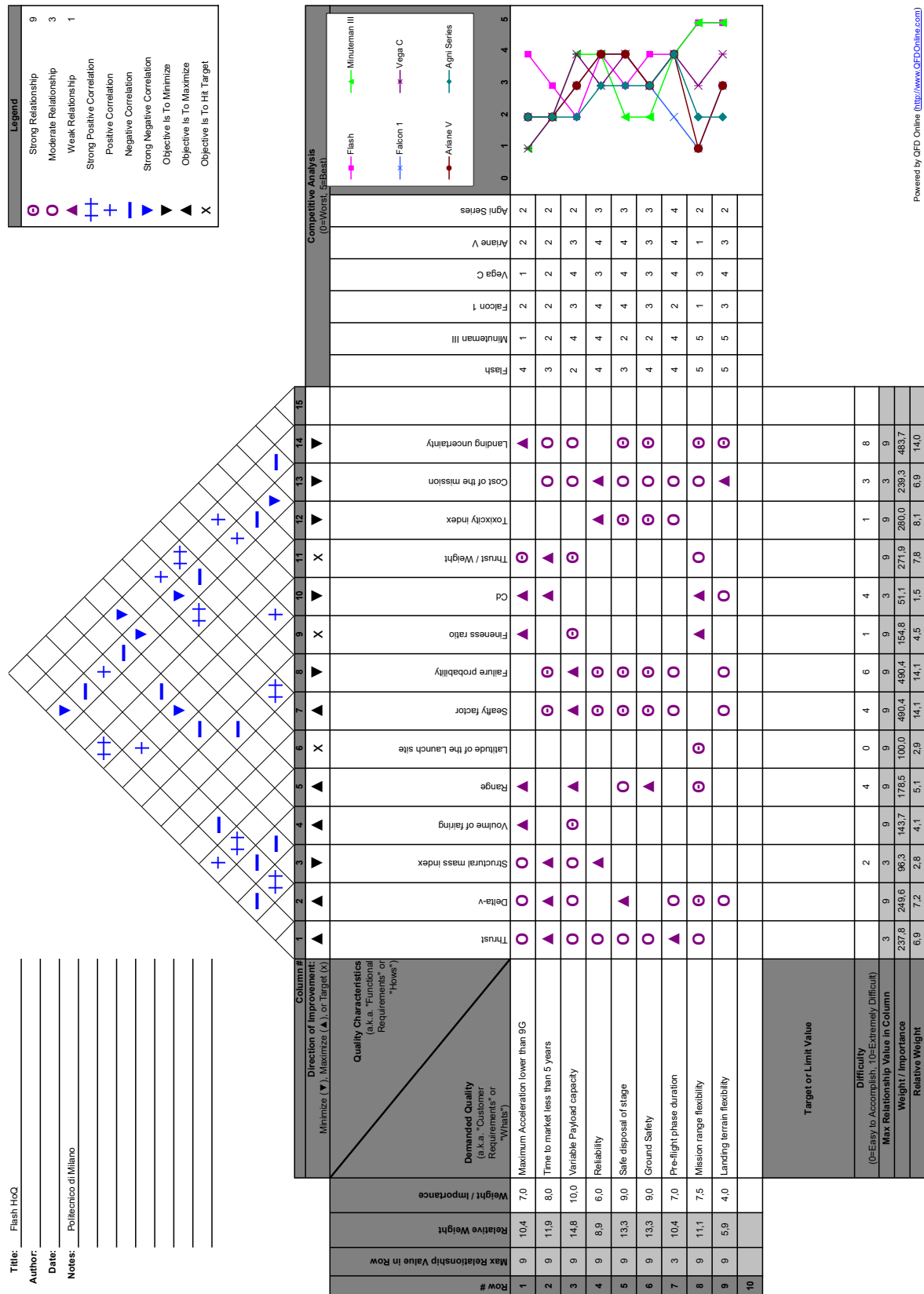


Figure 5.2: House of quality sheet

## Baseline

	STAGE 1	STAGE 2	STAGE 3
MER	39.96	35.89	22.93
$MER_{fairing}$	30.62		
Epsilon	0.1068	0.1019	0.0832
$(L/D)_{ratio}$	10.8690476	8.2900763	4.6412214
$Prop_{ratio}$	0.6235981	0.8931595	0.9167854

Table 5.2: Values of baselines for each stage

## TRL

---

Level	Description
1	Basic Principles
2	Application Formation
3	Technology Concepts & Research
4	Tech Development & Proof of Concept
5	Low Fidelity Component Testing (Labs)
6	System Integration & Flight Tests
7	Prototype Demonstration & Operation
8	Prototype Operation in Realistic Mission Scenario
9	UAS Mission Deployment
10	Fully Operational Status

Table 5.3: TRL criteria table [10]

**AD<sup>2</sup>****AD<sup>2</sup> level Description**

- 
- | AD <sup>2</sup> level | Description  |
|-----------------------|--|
| 9                     | Requires new development outside of any existing experience base. No viable approaches exist that can be pursued with any degree of confidence. Basic research in key areas needed before feasible approaches can be defined.  |
| 8                     | Requires new development where similarity to existing experience base can be defined only in the broadest sense. Multiple development routes must be pursued.  |
| 7                     | Requires new development but similarity to existing experience is sufficient to warrant comparison in only a subset of critical areas. Multiple development routes must be pursued.  |
| 6                     | Requires new development but similarity to existing experience is sufficient to warrant comparison on only a subset of critical areas. Dual development approaches should be pursued in order to achieve a moderate degree of confidence for success. (desired performance can be achieved in subsequent block upgrades with high degree of confidence.) |
| 5                     | Requires new development but similarity to existing experience is sufficient to warrant comparison in all critical areas. Dual development approaches should be pursued to provide a high degree of confidence for success.  |
| 4                     | Requires new development but similarity to existing experience is sufficient to warrant comparison across the board. A single development approach can be taken with a high degree of confidence for success.  |
| 3                     | Requires new development well within the experience base. A single development approach is adequate.   |
| 2                     | Exists but requires major modifications. A single development approach is adequate.  |
| 1                     | Exists with no or only minor modifications being required. A single development approach is adequate.  |
- 

Table 5.4: AD<sup>2</sup> criteria table [10]

## Cost and Business Analysis

Fixed Costs for Development	Working Hours	€/ hour	Nr. of people	Tot.
Project Manager	7500	40	2	600.000,00 €
Engineering	5000	35	35	6.125.000,00 €
Qualification	500	20	20	200.000,00 €
Supervisor	500	25	15	185.500,00 €
External Experts	150	35	3	15.750,00 €
	€/month			Nr. of Months
Loan	-	25000	45	1.125.000,00 €
Total Fixed Costs	-	-	-	8.253.250,00 €
Margin on the Total Cost	-	-	-	20 %
<b>Total Fixed Cost</b>				
<b>with Safety Margin</b>				<b>9.903.900,00 €</b>

Table 5.5: Fixed costs

		€/ kg	kg	Tot.
<b>Manufacturing</b>				
<b>Propellant</b>	HTPB	8	11914,175	95.313,40 €
	RP1	20	496,8291	9.936,58 €
	$H_2O_2$	0,5	331,2194	165,61 €
<b>Materials</b>	Alluminium 6061	2500	21551,95	53.879.875,00 €
	Carbon EPOXY	6,5	121,8	791,70 €
	Glass-S	10,6	498,875	5238,56 €
	Titanium	3,5	36	126,00 €
<b>Avionics</b>				
<b>and elettronics</b>	-	150	569,03	85.354,50 €
<b>Parachutes</b>				
	-	5	142,875	714,38 €
<b>Assembling</b>				
	-	20	30	1.500.000,00 €
<b>Operations</b>				
<b>Energy Bill</b>	-	-	-	20.000,00 €
<b>Building Loan</b>	-	-	-	220.000,00 €
<b>Launch Site Bill</b>	-	-	-	300.000,00 €
<b>Logistic</b>	-	-	-	40.000,00 €
<b>Permission</b>	-	-	-	40.000,00 €
<b>Total Operation Cost</b>	-	-	-	620.000,00 €
<b>Contingency</b>	-	-	-	15%
<b>Insurance</b>	-	-	-	15%

Table 5.6: Recurrent costs

<b>Total Manufacturing Cost</b>	<b>55.577.515,72 €</b>
<b>Total Operation Cost</b>	<b>806.000,00 €</b>
<b>Total Recurrent Cost</b>	<b>56.383.515,72 €</b>

Table 5.7: Total Recurrent costs

€/kg		Launch price	
35000		4300	
Nr of Launches per Year	Nr. of Year activity	Total Launches	Total Price
10	10	100	1.505.000,00€

Table 5.8: Launches Price

Actuation factor k=15%

Year	1	2	3	4
<b>NCF</b>	941.164.842,78 €	1.882.329.685,57 €	2.823.494.528,35 €	3.764.659.371,13 €
<b>NPV</b>	818.404.211,12 €	1.423.311.671,51 €	1.856.493.484,57 €	2.152.456.214,00 €
Year	5	6	7	8
NCF	4.705.824.213,92 €	5.646.989.056,70 €	6.588.153.899,48 €	7.529.318.742,26 €
<b>NPV</b>	2.339.626.319,56 €	2.441.349.203,02 €	2.476.731.075,53 €	2.461.347.652,70 €
Year	9	10		
<b>NCF</b>	8.470.483.585,05 €	9.411.648.427,83 €		
<b>NPV</b>	2.407.840.095,03 €	2.326.415.550,76 €		

Table 5.9: NCF and NPV

Where **NCF** is the Net Cash Flow and **NPV** is the Net Present Value which can be computed as:  $\frac{NCF_{year}}{(k + 1)^{year}}$

The **Net Actual Value** is then computed as:

$$NAV = \left( \sum_{years}^{years} NPV_{year} \right) - InitialInvestment$$

Where the **Initial Investment** is equal to 5.648.255.472,17 €. The **Return on Investment** correspond to 37.52%, while **Payback Time** is almost 3 years

## 5.2 Staging Appendix

The following equation represents the minimization function, denoted as  $J$ , with  $\Delta V$  serving as the constraint in this optimization algorithm. The parameter  $\eta$  acts as the reducing factor for the baseline propellant.

$$\begin{aligned} J &= \ln\left(\frac{m_0}{m_{\text{pay}}}\right) + \lambda \left( \Delta V - \sum_{i=1}^n c_i \ln(n_i) \right) \\ &= \sum_{i=1}^N \ln \left( \frac{(1 - \epsilon_{s,i}) n_i}{1 - \epsilon_{s,i} n_i} \right) + \lambda \left( \Delta V - \sum_{i=1}^n c_i \ln(n_i) \right) \end{aligned} \quad (5.1)$$

$$\begin{cases} \frac{dJ}{dn_i} = 0 \\ \frac{dJ}{d\lambda} = 0 \end{cases} \quad \begin{aligned} \Delta V &= \sum_{i=1}^N c_i \ln \left( \frac{c_i \lambda - 1}{\epsilon_{s,i} c_i \lambda} \right) \\ n_i &= \frac{c_i \lambda - 1}{\epsilon_{s,i} c_i \lambda} \end{aligned} \quad (5.2)$$

$$\eta = \frac{I_s \text{real}}{I_s \text{ideal}} \quad (5.3)$$

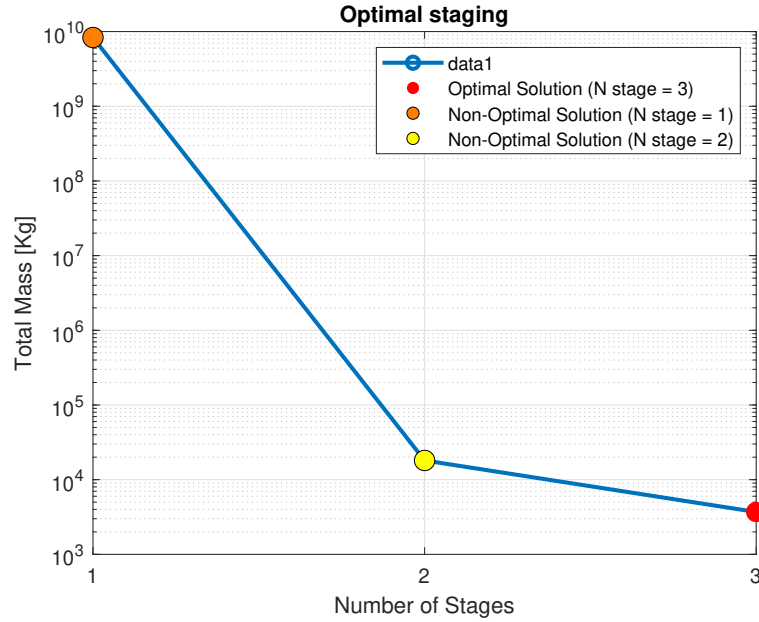


Figure 5.3: Optimal staging analysis

## 5.3 Aerodynamics Appendix

### Atmospheric Model

The U.S. Standard Atmosphere 1976 [4] is a model that provides a standardized representation of Earth's atmosphere from the ground up to 1000 kilometers. It gives atmospheric properties like temperature, pressure, density, and composition over a range of altitudes. Developed by NOAA, NASA, and the U.S. Air Force, this model is widely used in aerospace engineering. It's based on average atmospheric conditions and serves as a reference for comparing and analyzing atmospheric variations.

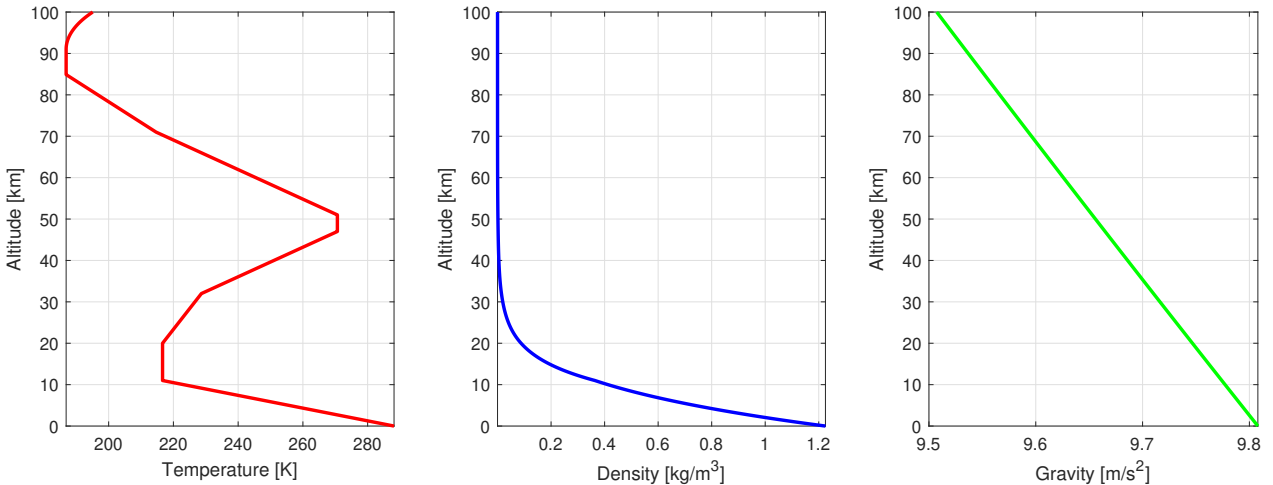


Figure 5.4: Temperature, density and gravity variation with altitude

### Paneling

In the left the Newton method while in the right the modified Newton method.

$$C_p = 2 \cdot \sin^2(\theta) \quad C_{p\text{modified}} = C_{p\text{max}} \cdot \sin^2(\theta) \quad (5.4)$$

$$C_{p\text{max}} = \frac{2}{M^2 \cdot \gamma} \left\{ \left[ \frac{(\gamma + 1)^2 \cdot M^2}{4 \cdot \gamma \cdot M^2 - 2 \cdot (\gamma - 1)} \right]^{\frac{\gamma}{\gamma - 1}} \cdot \left[ \frac{1 - \gamma + 2 \cdot \gamma \cdot M^2}{\gamma + 1} \right] - 1 \right\} \quad (5.5)$$

The equation here reported are the implementation of the paneling method, by assuming an angle  $\alpha$  between the i-direction and the incoming flux.

$$\mathbf{dF} = -C_p \cdot q \cdot A \cdot \hat{\mathbf{n}} \quad (5.6)$$

$$\mathbf{dF}_p = \mathbf{dF}_p \hat{i} + \mathbf{dF}_{a_p} \hat{j} + \mathbf{dF}_{a_p} \hat{k} \quad \mathbf{dD}_p = \mathbf{dF}_p \cdot \frac{\mathbf{V}_{\text{inf}}}{\sqrt{\mathbf{V}_{\text{inf}} \cdot \mathbf{V}_{\text{inf}}}} \quad (5.7)$$

$$\mathbf{dL}_p = \sqrt{\mathbf{dF}_p \cdot \mathbf{dF}_p - (\mathbf{dD})^2} \quad \mathbf{dM}_p = \mathbf{r}_p \times \mathbf{dF}_p \quad (5.8)$$

$$\hat{\mathbf{n}} = \frac{\mathbf{N}}{\sqrt{\mathbf{N} \cdot \mathbf{N}}} \quad \sin \theta = \frac{\mathbf{V}_{\infty}}{\mathbf{V}_{\infty}} \cdot \hat{\mathbf{n}} \quad \phi = \arccos \frac{\mathbf{v} \cdot \hat{\mathbf{n}}}{\mathbf{v}} \quad (5.9)$$

$$C_L = \frac{L}{q_{\infty} S} \quad C_D = \frac{D}{q_{\infty} S} \quad C_N = \frac{N}{q_{\infty} S} \quad C_A = \frac{A}{q_{\infty} S} \quad (5.10)$$

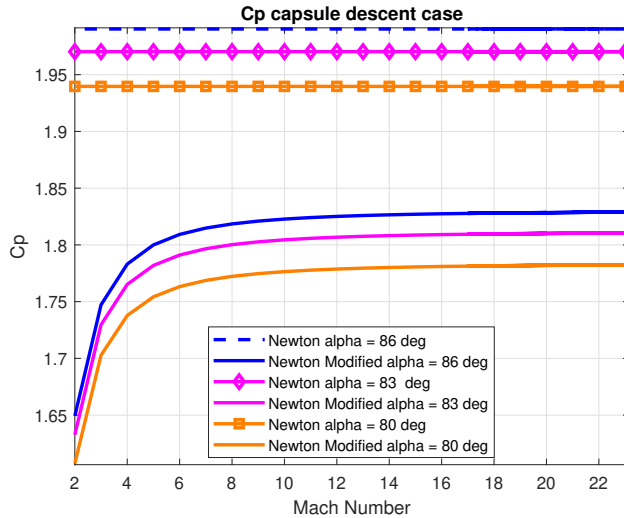


Figure 5.5: Pressure coefficients for Newton and modified Newton

- $C_p$  Newton method pressure coefficient.
- $C_{p,modified}$  modified Newton method pressure coefficient.
- $\theta$  angle between incoming flux and normal vector.
- $C_{p,max}$  pressure coefficient evaluated at the stagnation point.
- $\gamma$  specific heat ratio.
- $A$  elementary surface.
- $\hat{n}$  normal versor.
- $\mathbf{dL}_p, \mathbf{dD}_p$  Lift and Drag elementary force.
- $\mathbf{dM}_p$  elementary moment.

In the Figure 5.7 is depicted the implementation of the paneling method. In blue we have the incoming flux, while in black we have the normal forces.

Forces on Elementary Surfaces

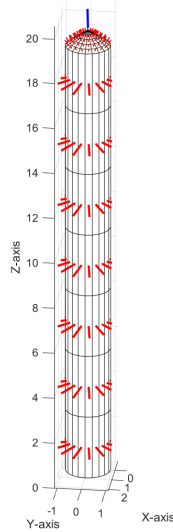


Figure 5.6: Normal vector forces

Forces on Elementary Surfaces

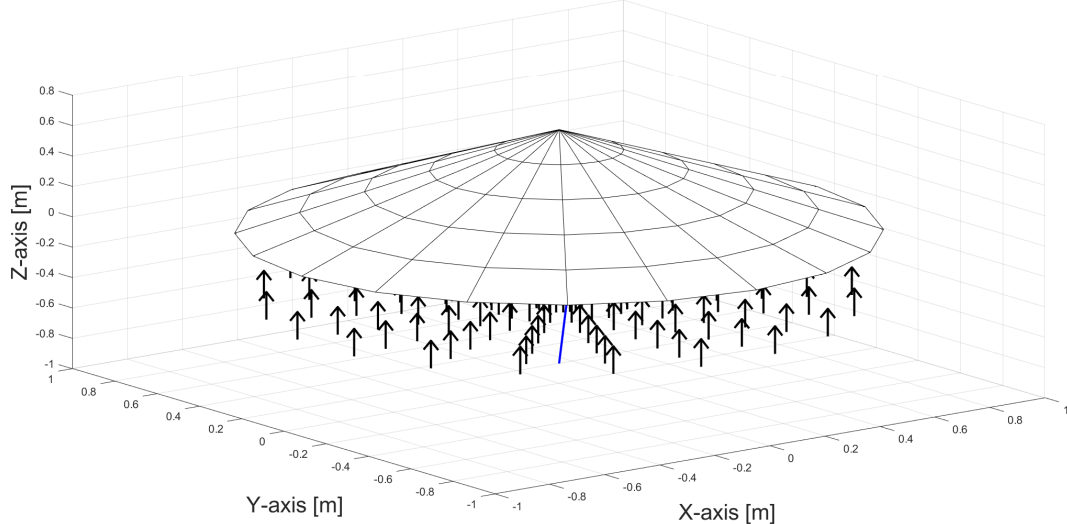


Figure 5.7: Normal forces during reentry

## Drag Coefficient Equations

The following equations were used to calculate the drag coefficient for each different contribution, the models of which are elaborated in the specified chapter section.

Body contributions :

$$C_{D0}^{\text{body, wave}} = \left( 1.586 + \frac{1.834}{M} \right) \cdot \left( \arctan \left( \frac{0.5}{\frac{L_n}{D_n}} \right) \right)^{1.69}$$

For a hemisphere,  $L_n/D_n = 0.5$

$$C_{D0}^{\text{body,friction}} = 0.053 \cdot \frac{L}{D} \cdot \left( \frac{M}{qL} \right)^{0.2}$$

	Subsonic regime	Supersonic regime
Powered phase	$C_{D0}^{\text{body,base}} = \left( 1 - \frac{A_e}{A_{ref}} \right) (0.12 + 0.13M^2)$	$C_{D0}^{\text{body,base}} = \left( 1 - \frac{A_e}{A_{ref}} \right) \frac{0.25}{M}$
Coast phase	$C_{D0}^{\text{body,base}} = 0.12 + 0.13M^2$	$C_{D0}^{\text{body,base}} = \frac{0.25}{M}$

Fins contributions :

$$C_{D0}^{\text{surf,friction}} = \eta_{\text{surf}} 0.0133 \left( \frac{M}{0.02l_q(3.28c_{\text{mac}})} \right)^{0.2} \left( \frac{S_{\text{surf}}}{S_{\text{ref}}} \right)^2$$

$$C_{D0}^{\text{surf,wave}} = \frac{\eta_{\text{surf}} 1.429}{M_{\text{ALE}}^2} \left[ \left( \frac{2.4M_{\text{ALE}}^2}{2.8M_{\text{ALE}}^2 - 0.4} \right)^{2.5} (1.2M_{\text{ALE}}^2)^{3.5} - 1 \right] \left( \frac{\sin^2 \delta_{\text{LE}} \cos \Lambda_{\text{LE}} 3.28t_{\text{mac}} b}{S_{\text{ref}}} \right)$$

- $\eta_{\text{surf}}$  is the number of surface planforms
- $\delta_{\text{LE}}$  is the leading edge section total angle;
- $\Lambda_{\text{LE}}$  is E is the leading edge sweep angle;
- $M_{\text{ALE}}$  is the Mach component normal to the surface's leading edge;
- $c_{\text{mac}}$  is the mean aerodynamic chord;
- $t_{\text{mac}}$  is the maximum thickness along MAC;

## Normal Coefficient Equations

The following equations were used to calculate the normal coefficient for each different contribution, the models of which are elaborated in the specified chapter section.

$$C_N^{\text{body}} = \sin 2\alpha \sin \frac{\alpha}{2} + \eta C_{DN} \frac{S_p}{S_{\text{ref}}} \sin^2 \alpha$$

$S_p$  is the major body planform area, and  $C_{DN}$  depends on the cross-flow Reynolds and Mach numbers. The selected values are as follows, based on reference [26]:  $\eta = 1.3398$ ,  $C_{DN} = 0.53$  [First].

Regime	$C_N$	$C_{N\alpha}$
$M < M_{cr}$	$\left( \frac{\pi A_{\text{surf}}}{2}  \sin \alpha' \cos \alpha' + 2 \sin^2 \alpha'  \right) \frac{S_{\text{surf}}}{S_{\text{ref}}} \quad \frac{\pi A_{\text{surf}} S_{\text{surf}}}{2 S_{\text{ref}}}$	
$M > M_{cr}$	$\left( \frac{4 \sin \alpha' \cos \alpha' }{\beta} + 2 \sin^2 \alpha' \right) \frac{S_{\text{surf}}}{S_{\text{ref}}} \quad \frac{4S_{\text{surf}}}{\beta S_{\text{ref}}}$	

- $\beta = \sqrt{|M^2 - 1|}$  is the Prandtl-Glauert factor;
- $M_{cr} = \sqrt{1 + \left(\frac{4}{A_{surf}}\right)^2}$  is the critical Mach number;
- $S_{surf}$  is the planform area (surface of two fins);
- $A_{surf} = \frac{b^2}{S_{surf}}$  is the surface aspect ratio;
- $\alpha_0 = \alpha + \delta$  is the sum of the body and the surface angles of attack.

## 5.4 Structure Appendix

For all stages the LSC will be composed of circular strips of explosive along the case. The outer diameter is similar to all three stages, thus the same number of LSC will be used. The explosive, similarly to [27] shall be around 4400 grains/feet. Consequently, three longitudinal struts (LSC) will be strategically positioned along the circumferential periphery of the propellant casing for each solid rocket stage.

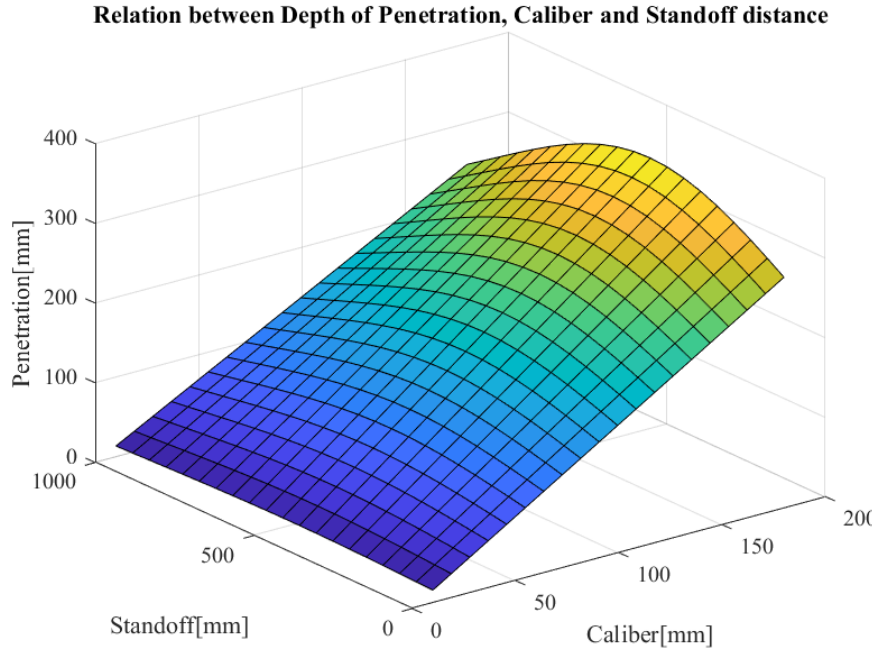


Figure 5.8: Relation between Depth of penetration, Caliber and Standoff distance [14]

$$H = \Phi k_1 k_2 k_{distance} \sqrt{\left(\frac{\rho_{jet}}{\rho_{target}}\right)} \quad (5.11)$$

$$k_{distance} = \frac{1}{1 + \left(\frac{S - 7C}{14C}\right)^2} \quad (5.12)$$

Where the terms represent [28]:

- $H$  = Depth of penetration
- $\rho_{jet}$  = Jet Density
- $\Phi$  = Warhead caliber
- $\rho_{target}$  = Target Density
- $k_1$  = Coefficient for jet length
- $S$  = Stand-off distance
- $k_2$  = Coefficient for target material
- $C$  = Caliber
- $k_{distance}$  = Coefficient for Stand-off distance

## 5.5 Propulsion Appendix

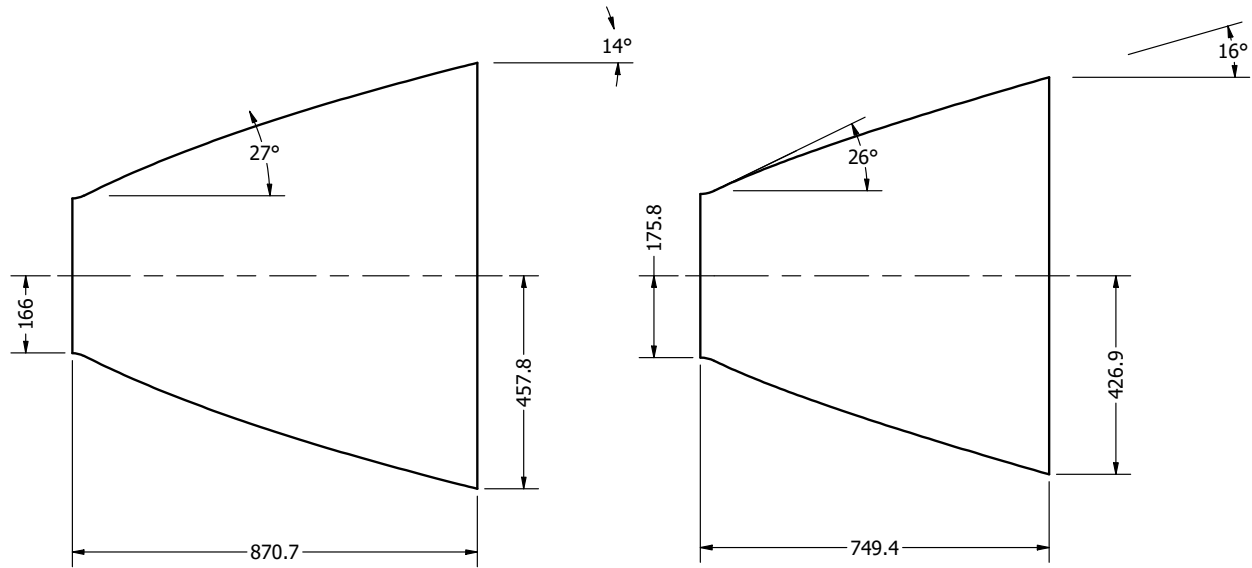


Figure 5.9: 1<sup>st</sup> stage nozzle before (left) and after (right) the modification

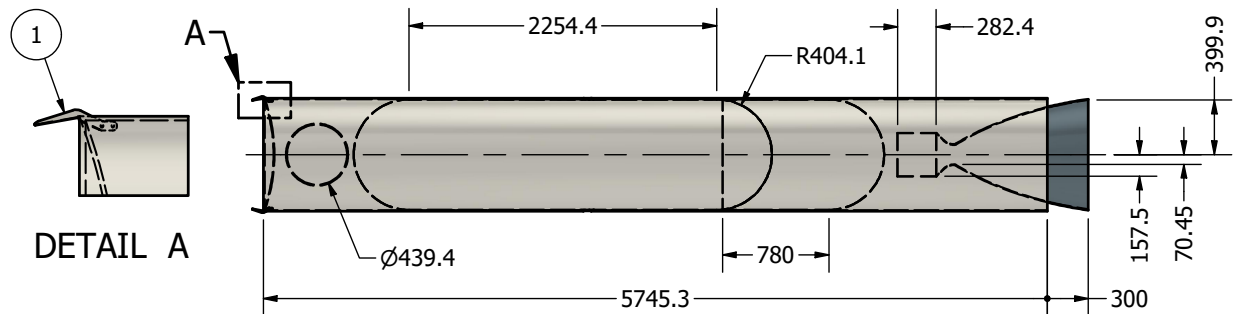
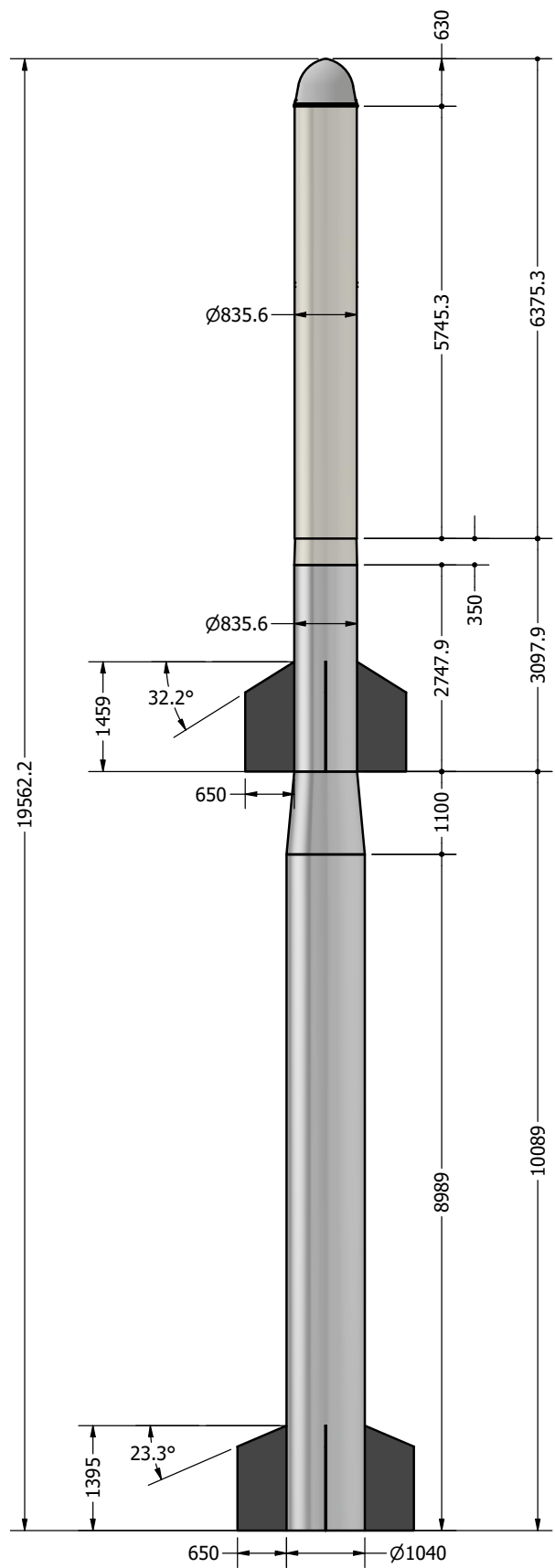
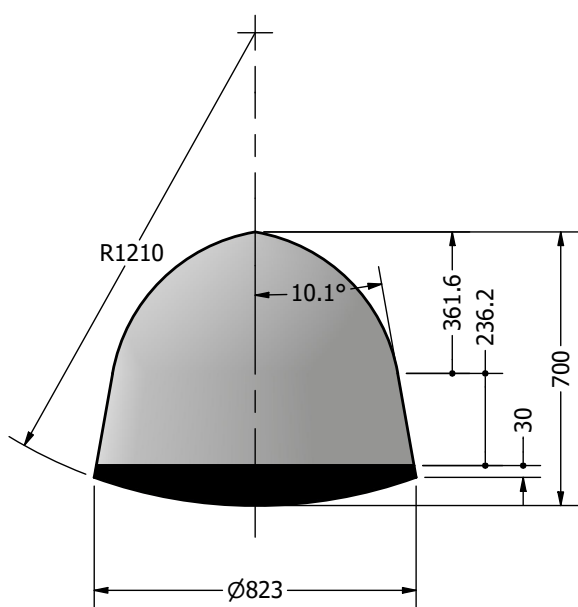


Figure 5.10: 3<sup>rd</sup> stage propulsion system: starting from left, the collet mechanism (1), the pressurising gas tank, oxidiser tank, fuel tank, combustion chamber and nozzle are shown in this order, together with their sizes.

## 5.6 Dimensions Appendix



(a) FLASH general dimensions



(b) Payload capsule general dimensions

## 5.7 Trajectory Appendix

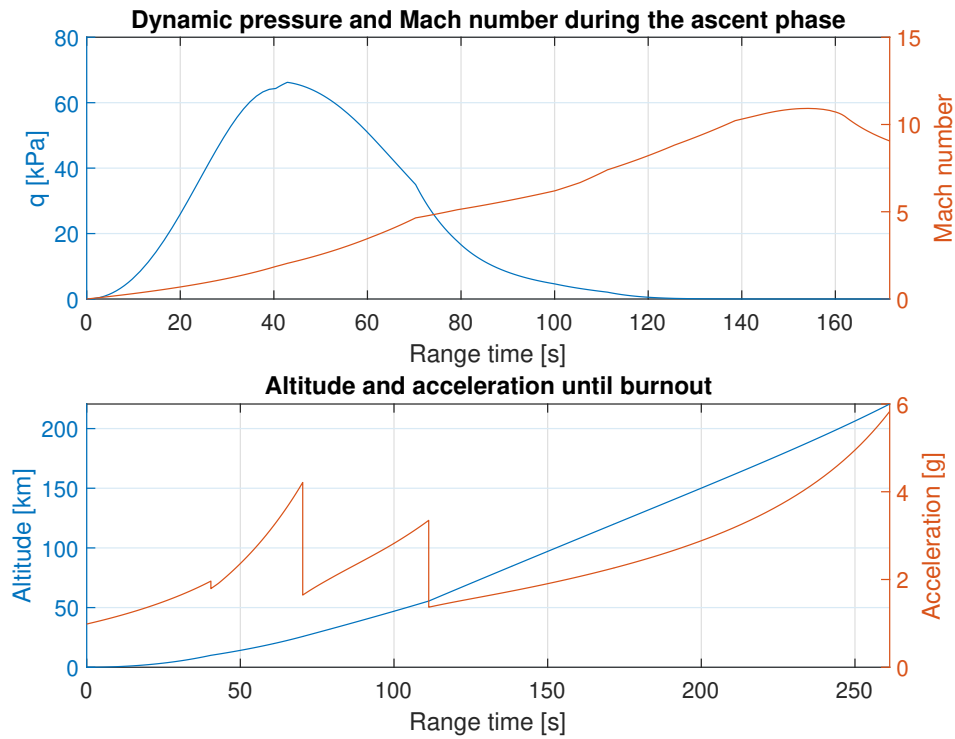


Figure 5.12: Time history for the ascent phase of the West Coast trajectory

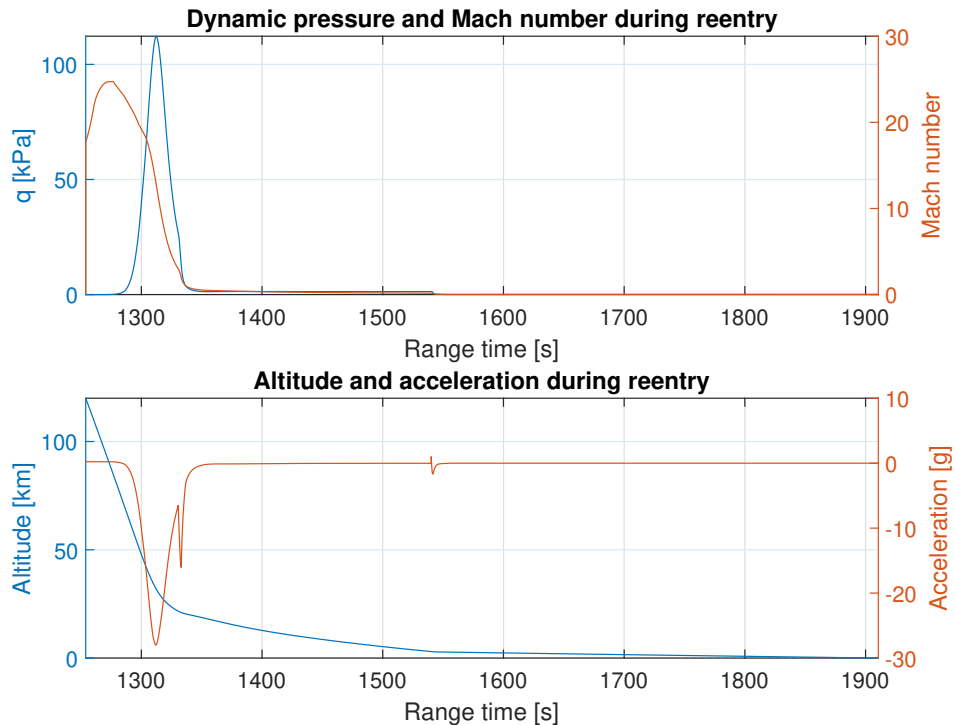


Figure 5.13: Time history for the descent phase of the West Coast trajectory

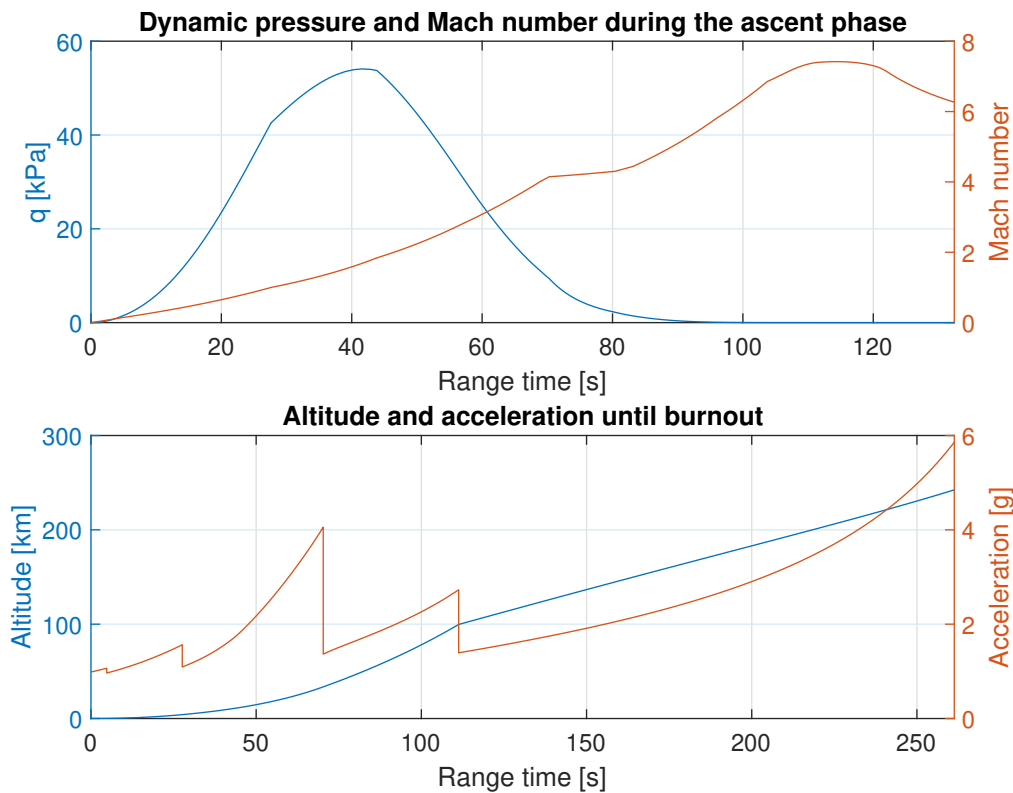


Figure 5.14: Time history for the ascent phase of the Midwest trajectory

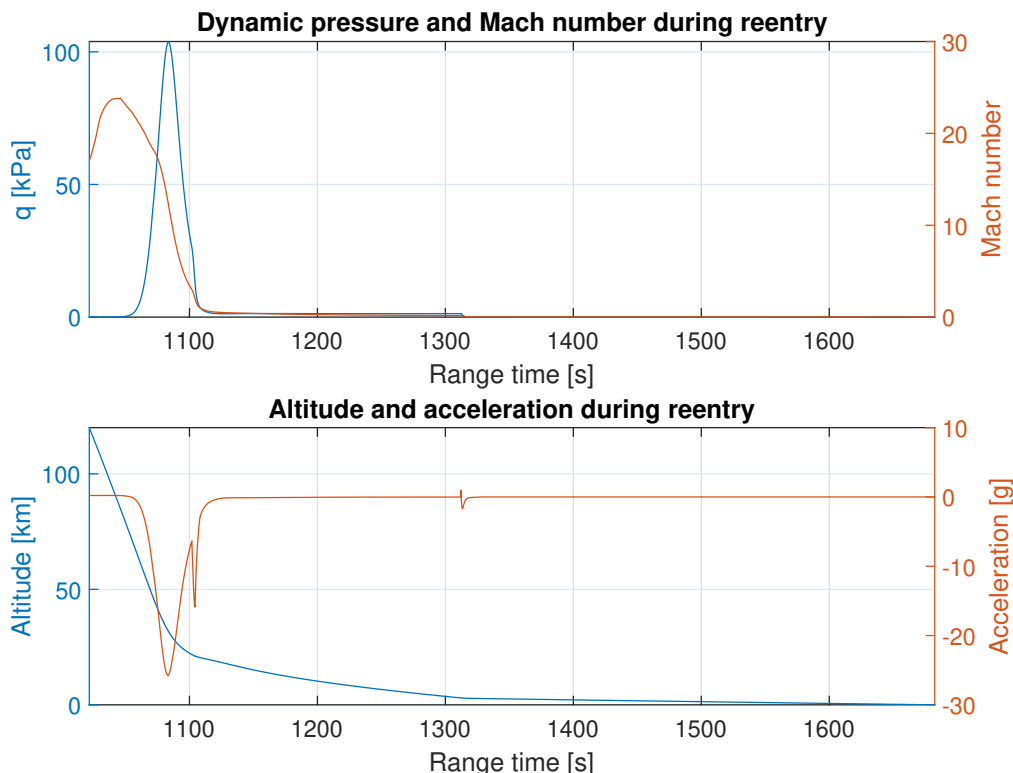


Figure 5.15: Time history for the descent phase of the Midwest trajectory

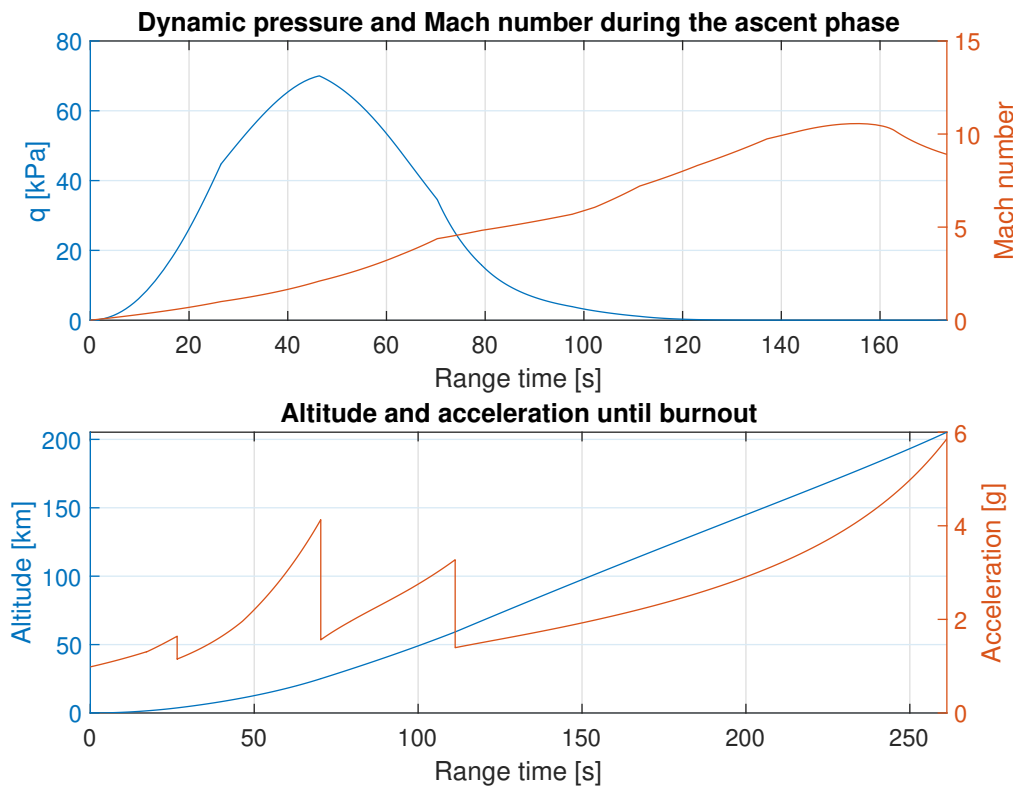


Figure 5.16: Time history for the ascent phase of the East Coast trajectory

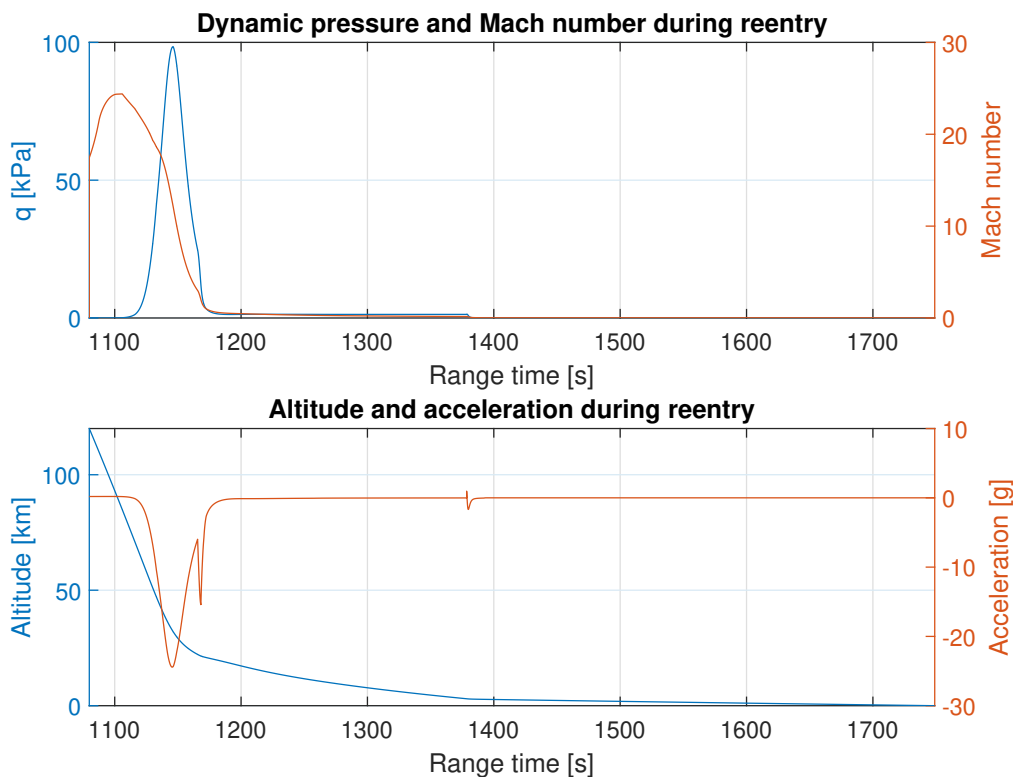


Figure 5.17: Time history for the descent phase of the East Coast trajectory

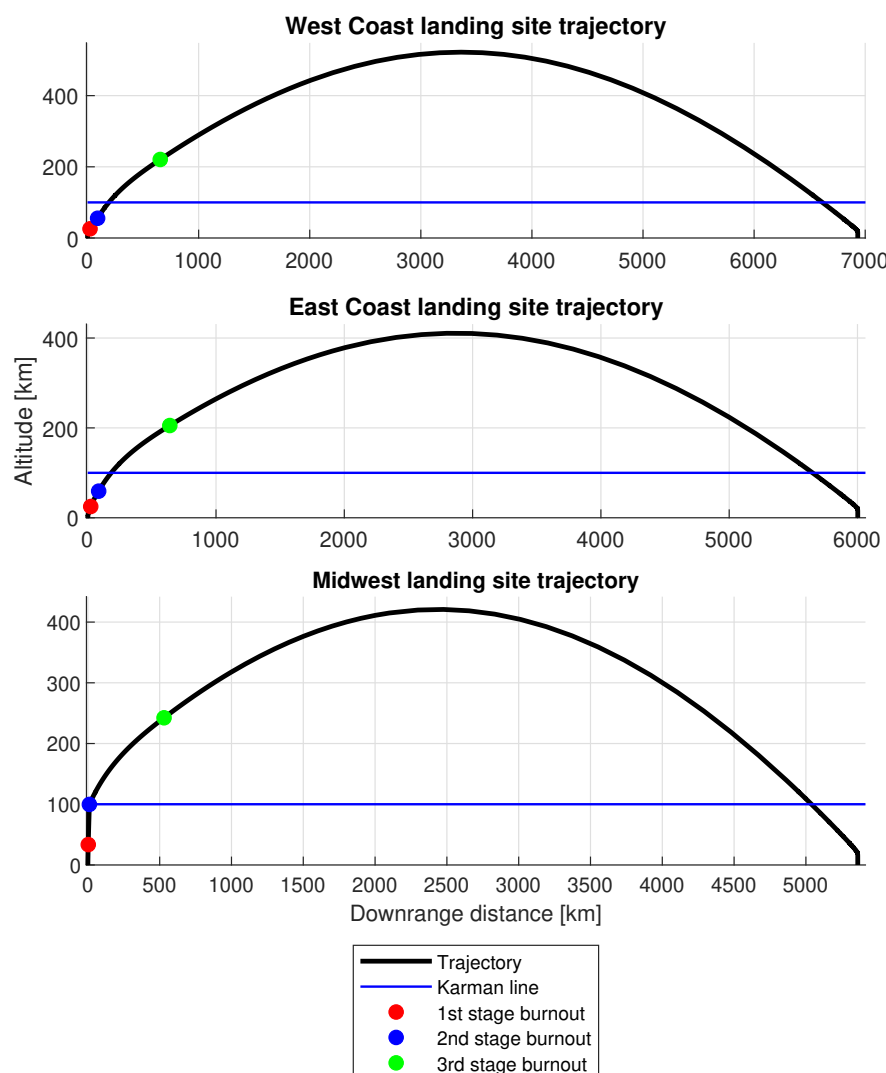


Figure 5.18: Trajectory simulation for each landing site

## 5.8 Atmospheric re-entry and landing Appendix

TYPE	CONSTRUCTED SHAPE		INFLATED SHAPE $\frac{D_p}{D_o}$	DRAG COEF $C_D$ RANGE	OPENING FORCE COEF $C_X$ (INF MASS)	AVERAGE ANGLE OF OSCILLATION, DEGREES	GENERAL APPLICATION	
	PLAN	PROFILE						
FLAT (FIST) RIBBON			1.00	0.67	0.45 TO 0.50	-1.05	0 TO ±3	DROGUE, DESCENT, DECLERATION, OBSCOLETE
CONICAL RIBBON			0.95 TO 0.97	0.70	0.50 TO 0.55	-1.05	0 TO ±3	DESCENT, DECLERATION, $0.1 < M < 2.0$
CONICAL RIBBON (VARIED POROSITY)				0.70	0.55 TO 0.60	1.05 TO 1.30	0 TO ±3	DROGUE, DESCENT, DECLERATION, $0.1 < M < 2.0$
RIBBON (HEMISPILO)			0.62	0.62	0.30 TO 0.46	1.00 TO 1.30	±2	SUPersonic. DROGUE. $1.0 < M < 3.0$
RINGSLOT			1.00	0.67 TO 0.70	0.56 TO 0.65	-1.05	0 TO ±5	EXTRACTION, DECLERATION, $0.1 < M < 0.9$
RINGSAIL			0.84	0.69	0.75 TO 0.85	-1.10	±5 TO ±10	DESCENT, $M < 0.5$
DISC-GAP-BAND			0.73	0.65	0.52 TO 0.58	-1.30	±10 TO ±15	DESCENT, $M < 0.5$

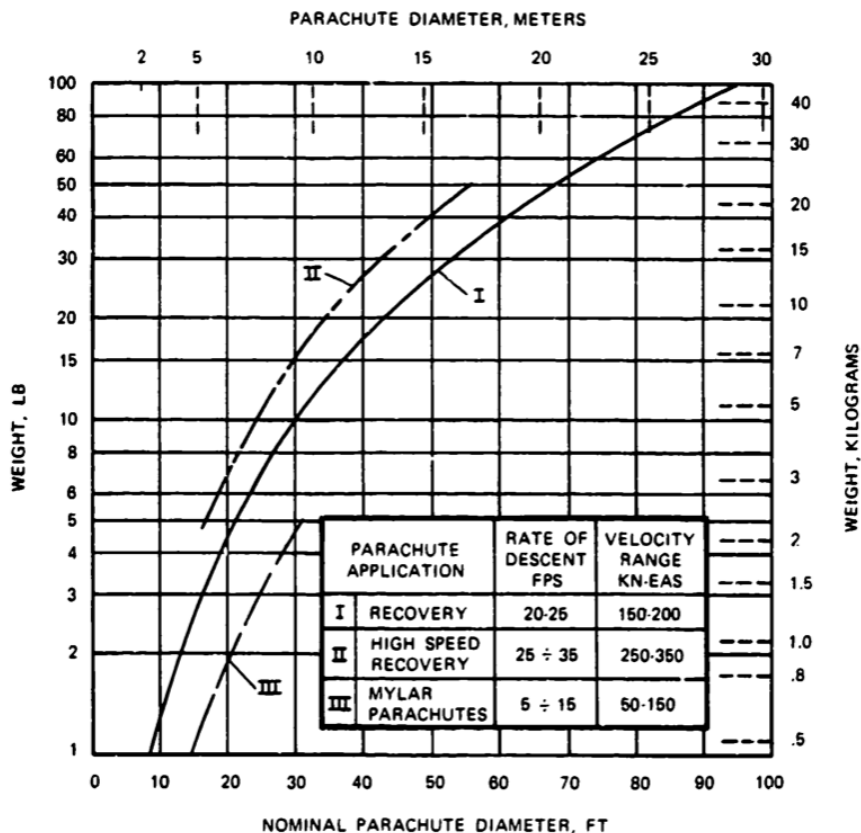
Figure 5.19: Tabulated  $C_D$  and  $C_X$  values [29]

FIGURE 6-62. Weight of Final descent Parachutes.

Figure 5.20: Parachute diameter and mass correlation [29]

Parachute type	Canopy fill constant, $n$		
	Reefed opening	Disreef opening	Unreefed opening
Solid flat circular	ID*	ID	8
Extended-skirt, 10%	16-18	4.5	10
Extended-skirt, full	16-18	7	12
Cross	ID	ID	11.7
Ribbon	10	6	14
Ringslot	ID	ID	14
Ringsail	7-8	2	7
Ribless guide surface	...	...	4-6

\* ID = Insufficient data available for meaningful evaluation.

Figure 5.21: Canopy Fill constant  $n$  for Various Parachutes Types [29]

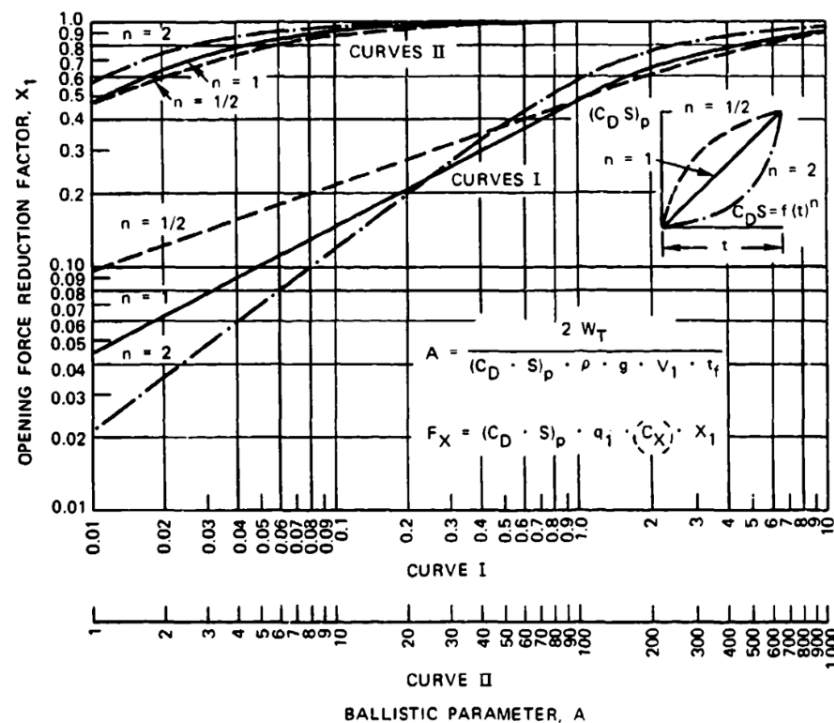


Figure 5.22: Opening-Force Reduction Factor  $X$  Versus Ballstic Parameter  $A$  [29]

## Montecarlo Analysis

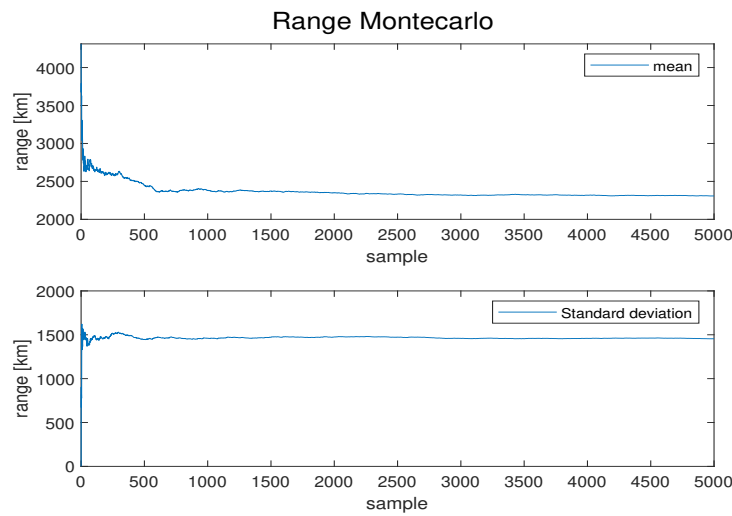


Figure 5.23: Montecarlo analysis for West landing site

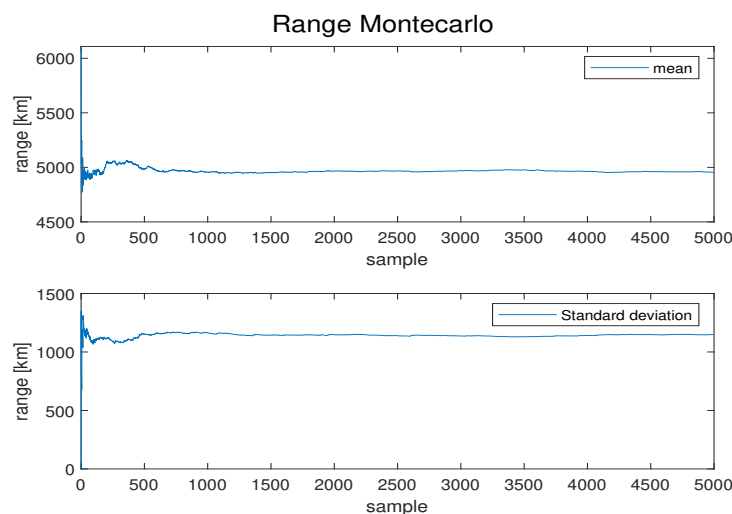


Figure 5.24: Montecarlo analysis for West landing site

## 5.9 Guidance Appendix

### Guidance equations

The equation of motion to be solved are:

$$\begin{bmatrix} \dot{\theta} \\ \ddot{\theta} \\ \dot{\alpha} \\ \dot{z} \\ \ddot{z} \end{bmatrix} = \begin{bmatrix} 0 & 1 & 0 & 0 & 0 \\ 0 & 0 & M_\alpha & 0 & 0 \\ -\frac{F}{mV} & 1 & -\frac{N_\alpha}{mV} & 0 & 0 \\ 0 & 0 & 0 & 0 & 1 \\ -\frac{F}{m} & 1 & -\frac{N_\alpha}{m} & 0 & 0 \end{bmatrix} \begin{bmatrix} \theta \\ \dot{\theta} \\ \alpha \\ z \\ \dot{z} \end{bmatrix} + \begin{bmatrix} 0 \\ M_\delta \\ \frac{T}{mV} \\ 0 \\ \frac{T}{m} \end{bmatrix} \delta + \begin{bmatrix} 0 \\ 0 \\ 0 \\ 0 \\ 0 \end{bmatrix} \quad (5.13)$$

where:

- $F = T_0 + T - A$
- $T_0$  is the nominal thrust
- $T$  is the thrust Vector magnitude
- $A$  is the axial force
- $N$  is the normal force
- $M$  is the torque
- $\alpha_{wind}$  is the angle of attack of the wind, which is considered constant and equal to  $5.73^\circ$
- $\theta$  is the pitch angle
- $z$  is the lateral deviation
- $\delta$  is the angle between the nominal thrust and the TVC which correspond to the control

All vectors and angle are referred to the following reference frame:

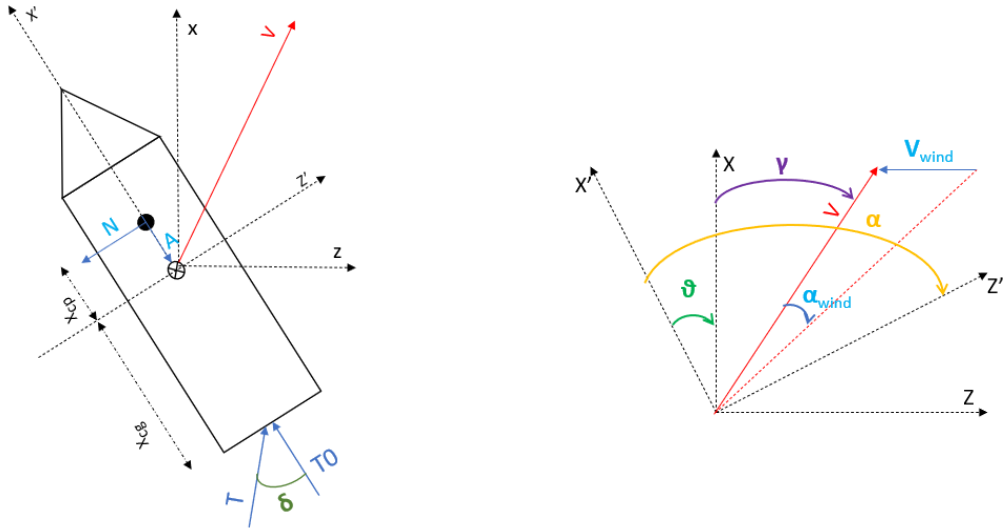


Figure 5.25: Reference Frame

## Control evolution

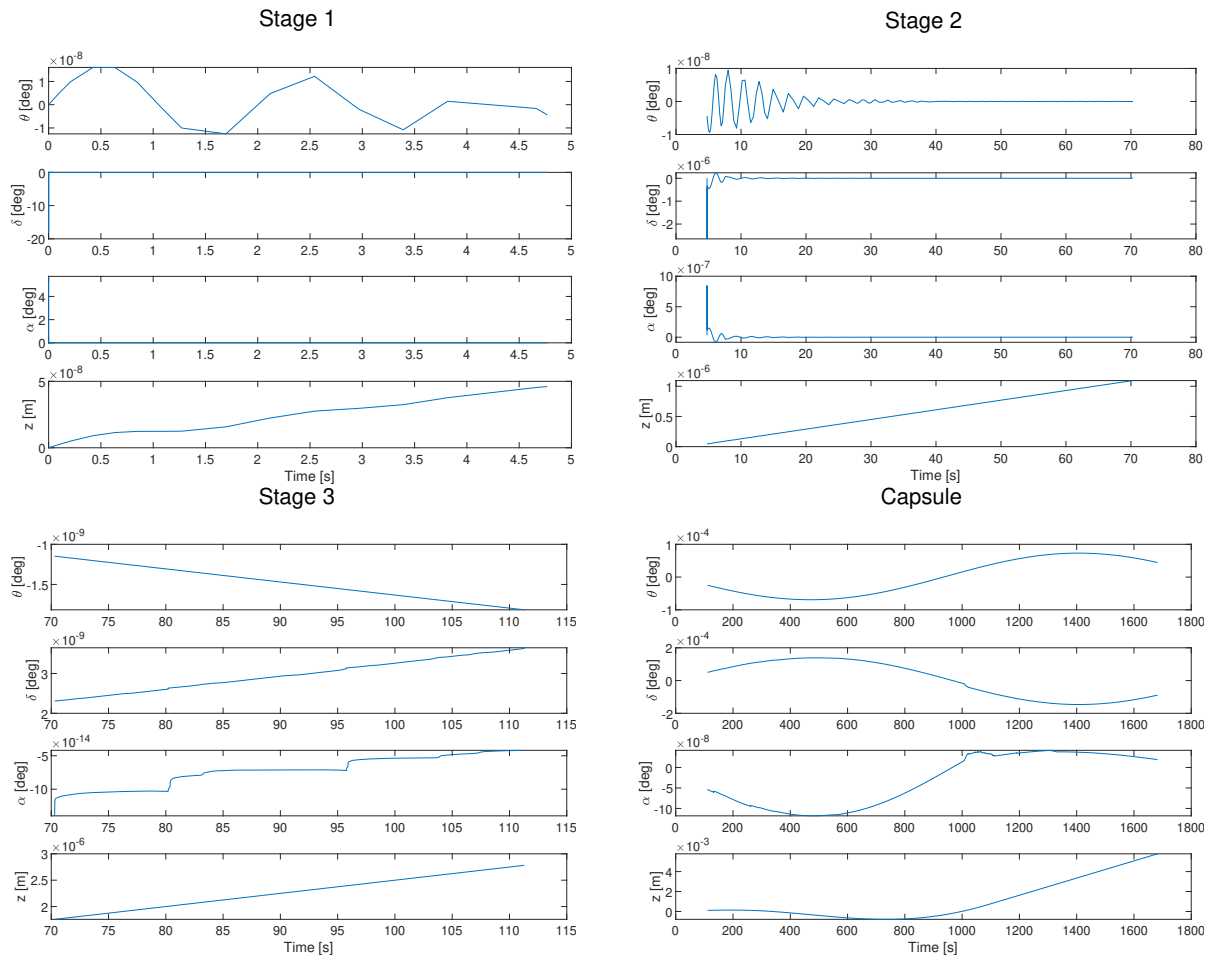


Figure 5.26: Control Evolution

# Bibliography

- [1] Marcello Spagnulo. *Elementi di management dei programmi spaziali*. Springer Science & Business Media, 2012.
- [2] Mark A. Berhow. *U.S. Strategic and Defensive Missile Systems 1950-2004*. Bloomsbury Publishing, 2005.
- [3] James C O'Halloran. "LGM-30G Minuteman III". In: *IHS Jane's Weapons: Strategic 2015-2016* (2015).
- [4] *U.S. Standard Atmosphere 1976*. Tech. rep. National Aeronautics and Space Administration (NASA), 1976.
- [5] Eugene L Fleeman. *Tactical Missile Design*. American Institute of Aeronautics and Astronautics, 2006.
- [6] James S Barrowman. *The practical calculation of the aerodynamic characteristics of slender finned vehicles*. Tech. rep. 1967.
- [7] M. Sforza. *Manned Spacecraft Design Principles*. 1st. Waltham, Massachusetts, USA: Elsevier, 2016.
- [8] Andreas Stamminger. "ATMOSPHERIC RE-ENTRY ANALYSIS OF SOUNDING ROCKET PAYLOADS". In: (2000).
- [9] Sampo Niskanen. "Development of an Open Source model rocket simulation software". Helsinki University of Technology, 2003.
- [10] Filippo Maggi. "Launch System Courses". 2023-2024.
- [11] Oscar Biblarz George P. Sutton. *Rocket Propulsion Elements, Ninth Edition*. 2017.
- [12] ATK. "ATK Space Propulsion Products Catalog". In: (2009).
- [13] D. Jeyakumar and K.K. Biswas. *STAGE SEPARATION SYSTEM DESIGN AND DYNAMIC ANALYSIS OF ISRO LAUNCH VEHICLES*. Tech. rep. 2003.
- [14] Deweyville Joseph J. Kliger. "SOLID ROCKET MOTORS INCLUDING FLIGHT TERMINATION SYSTEMS, AND RELATED MULTI-STAGE SOLID ROCKET MOTOR ASSEMBLES AND METHODS". In: (May 4, 2017).
- [15] Martin Marietta Aerospace3. "TITAN IIIE/CENTAUR D-1T SYSTEMS SUMMARY CONVAIR Aerospace Division of General Dynamics". In: (September 1973).
- [16] Marc Toussaint Jerry Haber. "Safety in Launch Operations". In: *Safety Design for Space Operations* (2013).
- [17] T. Britting, W. L. J. R. Toussaint, et al. "Selection Criteria for Parachutes of Student-Built Sounding Rockets". In: *Proceedings of the 4th Symposium on Space Educational Activities*. 2022, pp. 2–3.
- [18] Fruity Chutes. *Drogue and Pilot Parachute*. (Visited on 11/15/2022).

- [19] J. R. Cruz. *Parachute for Planetary Entry System, Part II*. Tech. rep. Exploration Systems Engineering Branch, NASA Langley Research Center, Sept. 2005.
- [20] John Martyn Schattyn. “Investigation of Ablation Materials”. Missouri School of Mines and Metallurgy, 1963, p. 39. URL: [https://scholarsmine.mst.edu/masters\\_theses/2816](https://scholarsmine.mst.edu/masters_theses/2816).
- [21] LOUIS B. WECKESSER WILLIAM C. CAYWOOD ROBERT M. RIVELLO. “TACTICAL MISSILE STRUCTURES AND MATERIALS TECHNOLOGY”. In: *Johns Hopkins APL Technical Digest* (1983).
- [22] Grant Henson. “Materials for Launch Vehicle Structures”. In: () .
- [23] National Aeronautics and Space Administration. *Parachute Testing for NASA’s Orion Spacecraft*. 2017. URL: [https://www.nasa.gov/wp-content/uploads/2017/12/orion\\_parachutes.pdf](https://www.nasa.gov/wp-content/uploads/2017/12/orion_parachutes.pdf).
- [24] Filippo Maggi. “Evaluating New Liquid Storable Bipropellants: Safety and Performance Assessments”. In: (2021).
- [25] NASA. “LIQUID PROPELLANTS SAFETY HANDBOOK”. In: (1965).
- [26] Leland H Jorgensen. *Prediction of static aerodynamic characteristics for space shuttle-like and other bodies at angles of attack from 0 deg to 180 deg*. Tech. rep. 1973.
- [27] Manuel G. Vigil. “Design of Linear Shaped Charges Using the LESCA Code”. In: (April 1990).
- [28] Åke Sivertun Frederick Johnsson Bengt Vretblad. “SHAPED CHARGE CALCULATION MODELS FOR EXPLOSIVE ORDNANCE DISPOSAL OPERATIONS”. In: (2012).
- [29] T. W. Knacke. *Parachute Recovery System Design Manual*. Naval Weapons Center China Lake, CA: Defense Technical Information Center, 1991.